SO(8) fermion dynamical symmetry and strongly correlated quantum Hall states in monolayer graphene

Lian-Ao Wu,[1,2,*] Matthew Murphy,[3,†] and Mike Guidry[3,‡]
[1]*IKERBASQUE, Basque Foundation for Science, 48011 Bilbao, Spain*
[2]*Department of Theoretical Physics and History of Science, Basque Country University (EHU/UPV), P. O. Box 644, 48080 Bilbao, Spain*
[3]*Department of Physics and Astronomy, University of Tennessee, Knoxville, Tennessee 37996, USA*
(Received 29 July 2016; revised manuscript received 22 January 2017; published 9 March 2017)

A formalism is presented for treating strongly correlated graphene quantum Hall states in terms of an SO(8) fermion dynamical symmetry that includes pairing as well as particle-hole generators. The graphene SO(8) algebra is isomorphic to an SO(8) algebra that has found broad application in nuclear physics, albeit with physically very different generators, and exhibits a strong formal similarity to SU(4) symmetries that have been proposed to describe high-temperature superconductors. The well-known SU(4) symmetry of quantum Hall ferromagnetism for single-layer graphene is recovered as one subgroup of SO(8), but the dynamical symmetry structure associated with the full set of SO(8) subgroup chains extends quantum Hall ferromagnetism and allows analytical many-body solutions for a rich set of collective states exhibiting spontaneously broken symmetry that may be important for the low-energy physics of graphene in strong magnetic fields. The SO(8) symmetry permits a natural definition of generalized coherent states that correspond to symmetry-constrained Hartree-Fock-Bogoliubov solutions, or equivalently a microscopically derived Ginzburg-Landau formalism, exhibiting the interplay between competing spontaneously broken symmetries in determining the ground state.

DOI: 10.1103/PhysRevB.95.115117

I. INTRODUCTION

Quantum Hall effects are characteristic of two-dimensional (2D) electron gases in strong magnetic fields. The integral quantum Hall effect (IQHE) [1] is explained in terms of weakly interacting electrons filling quantized Landau levels (LL) produced by application of a strong magnetic field perpendicular to the 2D gas [2]. In contrast, the fractional quantum Hall effect (FQHE) [3] can occur only as a result of strong electronic correlations in partially filled Landau levels [4].

Because of its massless chiral charge carriers and atomic-monolayer honeycomb lattice exhibiting sublattice, valley, and spin degeneracies, quantum Hall effects in graphene could be much richer than in the semiconductor 2D electron gas, where there is no crystal structure and the only degeneracies are those of the (nonrelativistic) Landau levels and spin. For graphene in strong magnetic fields, an integral quantum Hall effect [5,6] and a fractional quantum Hall effect [7–10] have been observed, with anomalous filling factors that reflect the unique degeneracies of the graphene electronic structure and the Dirac-like nature of its electrons.

The valley isospin and spin degrees of freedom imply that graphene in a strong magnetic field is described well by a low-energy Hamiltonian that commutes approximately with the generators of an SU(4) Lie algebra. This SU(4) symmetry allows classification of states in graphene, and can serve as the basis for computing explicit breaking of the SU(4) symmetry by small nonsymmetric terms in the effective Hamiltonian. However, there is growing evidence that many states observed in modern experiments cannot be described by explicit breaking of SU(4). For example, the ground state of graphene in a magnetic field at low temperature exhibits a rapid increase of the longitudinal resistance R_{xx} above a critical magnetic field B_c [11]. The value of B_c decreases for increasingly cleaner samples, indicating that the resistance is not caused by impurity scattering but instead is intrinsic to the state itself [12]. In quantum Hall systems the currents are carried by edge states, so this insulating ground state must correspond to an emergent state that does not support edge currents produced by *spontaneous* (not explicit) breaking of the SU(4) symmetry.

Thus the approximate SU(4) symmetry of graphene can suggest possible low-energy collective modes exhibiting spontaneously broken symmetry that are important for the properties of graphene in a magnetic field, but the SU(4) symmetry alone cannot determine which of these modes is the ground state. Until now, those broken-symmetry modes have been addressed quantitatively by numerical simulations employing limited numbers of states and particles, or by effective low-energy field-theory approximations. These calculations find various possible low-energy collective states resulting from spontaneous breaking of the SU(4) symmetry with very similar energies. Thus they have been unable to give a definitive answer to the nature of the insulating ground state. Let us note that other approaches to the problems addressed here have been proposed (for example, Refs. [13–15]). However, the present discussion will concentrate on methods based on approximate SU(4) symmetry of the Hamiltonian.

An alternative and potentially more powerful application of symmetries has been employed extensively in both nuclear structure and condensed matter physics [16–20]. This *fermion dynamical symmetry method* truncates the Hilbert space to a tractable collective subspace by positing a highest symmetry associated with the physical operators for the system, and constructing effective Hamiltonians from polynomials in the Casimir invariants of the highest symmetry's subgroup chains. In this approach it is possible not only to classify low-energy

*lianaowu@gmail.com
†mhatt511@gmail.com
‡guidry@utk.edu

collective modes, but to solve analytically for the properties of these modes and to determine which lie lowest in energy, either exactly in particular symmetry limits, or approximately using generalized coherent state methods.

In an earlier paper the first application of fermion dynamical symmetry methods to graphene was introduced and applied to determining the ground state in strong magnetic fields [21]. This paper develops the full dynamical symmetry formalism upon which Ref. [21] rests. It will be shown that the highest symmetry is SO(8), with its generators identifiable with particle-hole and pairing degrees of freedom that have been discussed previously in the physics of graphene. This symmetry will be shown to be isomorphic to an SO(8) symmetry used extensively in nuclear structure physics, which permits already-developed mathematics to be appropriated for the graphene problem, and suggests instructive physical analogies between two very different physical systems. A generalized coherent state approximation will be introduced that corresponds to a Hartree-Fock-Bogoliubov (HFB) formalism subject to SO(8) symmetry constraints. This permits quantitative evaluation of energy surfaces associated with spontaneously broken symmetry.

The SO(8) highest symmetry will be shown to have an SU(4) subgroup that recovers the known physics of SU(4) quantum Hall ferromagnetism as a special case, but implies in the more general case new low-energy physics that transcends SU(4) quantum Hall ferromagnetism. Hence a solvable and physically illuminating approach to the rich low-energy structure of undoped graphene in strong magnetic fields will be proposed that reproduces known physics, but also suggests testable new physics in this complex system.

II. OVERVIEW OF PAPER

The organization of our presentation is as follows. A brief overview of the structure of graphene in a magnetic field and associated quantum Hall states will be given in Secs. III–V, with emphasis on those aspects important for the material of this paper. Then what is presently known about symmetries for graphene states in a magnetic field, in particular SU(4) quantum Hall ferromagnetism, is reviewed in Sec. VI. This will complete the survey of known physics required as background for this paper.

In Sec. VII, the essential idea of the new approach to collective states in graphene in terms of fermion dynamical symmetries will be introduced and related to standard SU(4) quantum Hall ferromagnetism. Section VIII is pivotal: there the mathematical proof will be given that the structure of the fermion dynamical symmetry wave function is equivalent to that of wave functions employed in more traditional discussions of graphene quantum Hall states, even though it looks very different superficially. In Sec. IX, it will then be shown in outline how this implies that the new fermion dynamical symmetry methods recover in one limit standard SU(4) quantum Hall ferromagnetism, but open the possibility of new physics beyond the SU(4) symmetry that can be obtained analytically using the SO(8) Lie algebra. This is the most important finding of this paper, and the remaining sections will elaborate on this theme.

In Secs. X–XIII, it will be shown that in a particular representation the fermion dynamical symmetry proposed for graphene is isomorphic to an SO(8) dynamical symmetry already well known in nuclear structure physics. It will then be shown in Sec. XIV that in a different representation more naturally adapted to the physics of graphene many already-known results from the nuclear SO(8) can be adapted immediately to the graphene problem (since matrix elements calculated from Lie algebras are invariant under a change of representation for the algebra). This will complete the development of the formal SO(8) description of graphene in a magnetic field. The remainder of the paper will entail finding solutions for the corresponding equations and interpreting them physically.

In Secs. XV–XVIII, the methods of Lie algebras will be used to obtain analytical solutions for the graphene SO(8) states, first for exact many-body solutions in the dynamical symmetry limits, and then for approximate Hartree-Fock-Bogoliubov solutions obtained using generalized coherent state methods valid even when dynamical symmetries are broken. These methods will then be used to investigate possible low-lying collective states and quantum phase transitions among them for graphene in a magnetic field in Sec. XIX. Section XX then presents an extensive discussion of the potential implications of these findings for understanding the nature of the ground state for graphene in a magnetic field, possible experimental tests, and potential shortcomings of our new methods. Finally, a summary is given in Sec. XXI.

III. LATTICE STRUCTURE OF GRAPHENE

Comprehensive reviews of graphene physics may be found in Refs. [22,23]. The presentation here will recall only a select set of features that will be relevant for subsequent discussion. Undoped graphene is a two-dimensional semiconductor with zero band gap. It has a bipartite honeycomb lattice structure that corresponds to two interlocking triangular sublattices, labeled A and B. The twofold degree of freedom specifying whether an electron is on the A sublattice or B sublattice is a spinlike quantum number termed the *sublattice pseudospin*. The dispersion of energy with momentum for undoped graphene in the absence of a magnetic field is illustrated in Fig. 1.

The two inequivalent points K and K' are not connected by reciprocal lattice vectors. The corresponding twofold K degree of freedom is commonly termed the *valley isospin* because of the valleylike structure in the dispersion of Fig. 1 around the K points. For brevity, the valley isospin will sometimes be termed simply *isospin.*

Near the *Dirac cones* (inset to Fig. 1), the dispersion is linear, the density of electronic states tends to zero, and the electrons are described by a massless Dirac equation in which the Fermi velocity plays the role that the speed of light would play in an actual relativistic system. Thus the low-energy electrons for undoped graphene in zero magnetic field behave to good approximation as *massless chiral fermions,* with the chirality representing the projection of the sublattice pseudospin on the direction of motion. The vanishing of the density of states at the Dirac point (Fermi surface) implies that

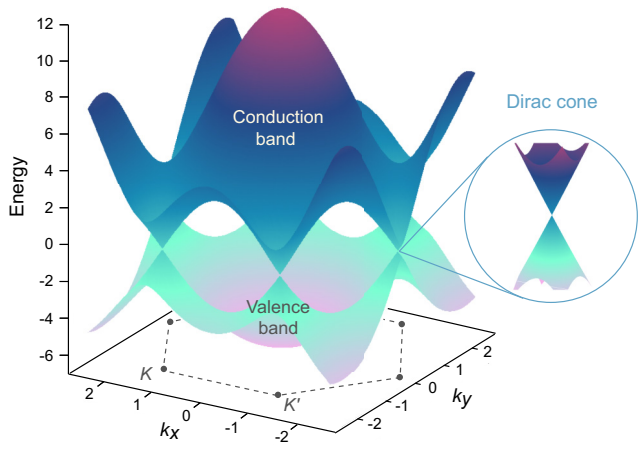

FIG. 1. Electronic dispersion of graphene calculated in a tight-binding model with no magnetic field. Two inequivalent points in the Brillouin zone are labeled K and K'. Near these K points the dispersion becomes linear, leading to *Dirac cones,* as shown in the expanded view. For undoped graphene, the Fermi surface lies at the apex of the cones, where the level density vanishes and the effective electronic mass tends to zero. Thus low-energy electrons are governed approximately by a Dirac equation for massless electrons.

the transport properties are different from either a metal or a semiconductor.

IV. GRAPHENE IN A MAGNETIC FIELD

Our interest will be primarily low-energy states in a strong magnetic field. For noninteracting electrons, the quantized levels may be found by solving the Dirac equation for massless fermions with a vector potential appropriate to the applied magnetic field. The dispersion of energy with magnetic field strength for massless Dirac electrons is illustrated in Fig. 2(a). Consider the $\nu = 0$ state, which corresponds to half-filling of the fourfold-degenerate $n = 0$ LL in graphene, as illustrated in Fig. 2(b). The graphene honeycomb lattice is bipartite, with A and B sublattices. The $n = 0$ LL is located exactly at the Dirac point corresponding to $\epsilon = 0$. For low-energy excitations in each valley labeled by K or K', the intervalley tunneling may be ignored and the electrons in the valley reside entirely on either the A or B sublattice. Hence, for the $n = 0$ LL labeling with the valley isospin (indicating whether the electron is in a K or K' valley) is equivalent to labeling with the sublattice pseudospin (indicating whether the electron is on the A or B sublattice). The resulting state is reminiscent of a Néel state with spins on two different sublattices, with a Néel order defined by the difference in spins on the A and B sublattices.

V. QUANTUM HALL EFFECTS IN GRAPHENE

A quantum Hall effect is signaled by a plateau in the Hall conductance σ_{xy} having quantized values

$$\sigma_{xy} = \frac{\nu e^2}{h}, \tag{1}$$

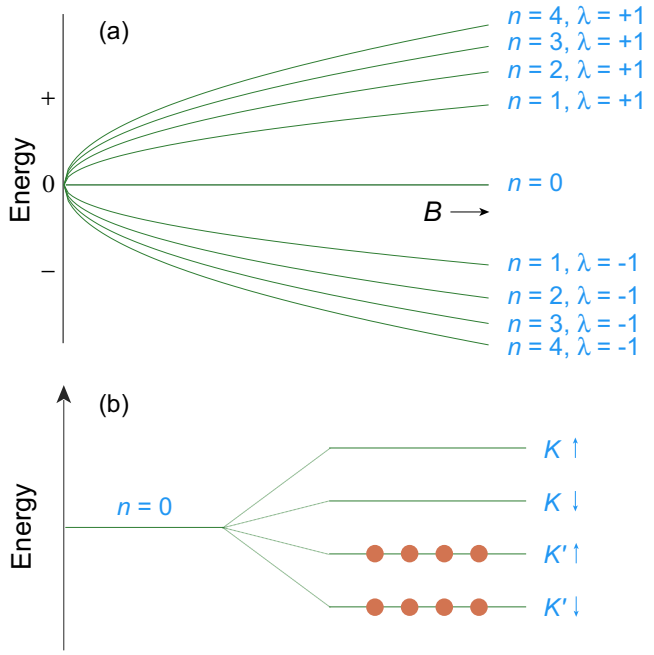

FIG. 2. (a) Relativistic dispersion for massless Dirac electrons as a function of magnetic field strength B. States are labeled by a principle quantum number n and a quantum number λ indicating particlelike (+) and holelike (−) states. Each Landau level labeled by n has a high orbital degeneracy Ω_k [see Eq. (21)], and an additional fourfold degeneracy associated with spin and valley isospin. (b) One configuration for occupation of the $n = 0$ Landau level in monolayer graphene. The splitting and occupation are schematic only. The ground state would be a superposition of such configurations and in the SU(4) symmetry limit (which obtains for Coulomb-only interactions) the four levels shown labeled by valley K or K' and spin up or down would be degenerate. In realistic cases the splitting often is small, suggesting approximate SU(4) symmetry.

where the *filling factor* ν is defined by

$$\nu = \frac{n_e}{n_B} = \frac{h n_e}{eB}, \tag{2}$$

with n_e the charge-carrier density, B the magnetic field strength, and $n_B = B/(h/e)$ the magnetic flux density in units of the fundamental flux quantum h/e. These plateaus indicate formation of an *incompressible quantum liquid.* This is a compact way to say that the ground state is separated from excited states by an *energy gap,* which inhibits compression because of the energy required for excitation across the gap.

A. Integral quantum Hall states

The integral quantum Hall effect (IQHE) in graphene is similar to the integral quantum Hall effect for nonrelativistic electrons in that it corresponds to the formation of incompressible states resulting from the complete filling of Landau levels by weakly interacting electrons. However, there are two important differences between the IQHE states observed in graphene and those observed in conventional 2D semiconductor heterostructures.

(1) In addition to the twofold spin degeneracy (in the absence of Zeeman splitting), there is a twofold valley

degeneracy associated with the distinct K and K' points in the first Brillouin zone. Thus the filling factor changes in steps of four between plateaus in the Hall resistance for graphene.

(2) For graphene, the filling factor ν defined in Eq. (2) vanishes at the Dirac point for particle-hole symmetric half-filling of the graphene lattice, since the electron density n_e tends to zero there. Hence, in the absence of a Zeeman effect or strong electronic correlations, there is no integral quantum Hall effect in graphene for $\nu = 0$.

In graphene, the analog of the integral quantum Hall effect was first observed at filling factors

$$\nu = \pm 2, \pm 6, \pm 10, \ldots \tag{3}$$

by sweeping the field or the carrier density through the Landau levels [5,6]. This implies Hall resistance quantization for filling factors in the sequence

$$\nu = \frac{hn_e}{eB} = 4\left(n + \frac{1}{2}\right) = 4n + 2, \tag{4}$$

where n_e is the charge carrier density and n is the Landau level index [5,9]. This sequence is quite different from the integral quantum Hall effect sequence observed in other 2D electron gases. However, it likely results from the same basic physics as the normal IQHE, modified by the fourfold spin-valley degeneracies of noninteracting, massless Dirac electrons.

The period $\Delta\nu = 4$ in Eq. (4) is a consequence of the approximate fourfold degeneracy of the graphene Landau level, and the added $1/2$ (which is not present in nonrelativistic 2D systems) is a Berry phase effect that results from the special status of the $n = 0$ state for massless Dirac fermions: a quantum phase arises at the band degeneracy point associated with precession of the pseudospinor describing the twofold sublattice degree of freedom, which modifies the quantization condition for electronic orbits [6,24,25]. The fourfold near degeneracy of the Landau level follows because the Zeeman energy is small compared with the interaction energy, and the pseudospin degree of freedom representing the two inequivalent Dirac cones at the corners of the Brillouin zone (K and K') does not couple to external fields if the two sublattices are equivalent.

B. Fractional quantum Hall states

Because of the Dirac-cone dispersion with the Fermi level located at the apex of the cones (see Fig. 1), low-energy excitations in graphene occur in regions of reduced electron density, which disfavors electron correlations. But by placing a strong perpendicular magnetic field on the system the resulting Landau quantization (corresponding semiclassically to requiring that an integral number of deBroglie wavelengths wrap around a cyclotron orbit, and implying that an integral number of magnetic flux quanta pass through the area bounded by the orbit) leads to a bunching of levels into regions of locally high degeneracy separated by gaps. These regions of locally high level density may exhibit conditions more favorable for the development of strong correlations between electrons.

Landau levels (LL) become strongly correlated when inter-LL excitations are of sufficiently high energy that they may be neglected and the low-energy excitations involve only intra-LL transitions. Then the kinetic energy of the LL is a constant that can be omitted. This limit of strong electronic correlations has two important physical implications. (1) The approximate fourfold spin-valley degeneracy of the graphene Landau levels leads to quantum Hall ferromagnetic states that will be discussed further below. (2) The strong correlations can produce incompressible states at partial filling of the LL that are reminiscent of the fractional quantum Hall effect (FQHE) in semiconductor devices.

After the discovery of the integral quantum Hall effect in graphene, experiments performed at higher magnetic field strengths observed quantum Hall states at filling factors $0, \pm 1, \pm 4$. The ± 4 states are thought to be the result of single-particle Zeeman splitting of the Landau levels but the states at filling factors $0, \pm 1$ are thought to be caused by electron-electron interactions breaking degeneracies of the $n = 0$ Landau level [7]. The structure of these incompressible states formed by electron-electron and electron-lattice correlations in partially filled Landau levels are the primary focus of this paper.

VI. QUANTUM HALL SYMMETRIES IN GRAPHENE

In the normal two-dimensional electron gas produced in semiconductor devices, the Landau levels can contain eB/h states, where e is the electronic charge and B is the magnetic field. As has been seen, in graphene there is an additional fourfold degeneracy associated with the spin and valley degrees of freedom. It is common to unite these four degrees of freedom in terms of an SU(4) symmetry that is termed *quantum Hall ferromagnetism (QHFM).*

A. SU(4) quantum Hall states

SU(4) symmetry for graphene in a strong magnetic field is expected when all four spin and valley levels are degenerate. Two conditions must be satisfied for this condition to be fulfilled. (1) Landau-level mixing caused by inter-LL electronic transitions must be negligible. (2) Perturbations within a single LL that break the fourfold spin-isospin symmetry must be small. The resulting theory predicts quantum Hall states that have no analog in semiconductor heterostructures.

The two-dimensional electronic spin degree of freedom and the two-dimensional electronic valley (K) degree of freedom are most elegantly expressed in terms of independent spin and valley isospin states. For the spin, introduce the Pauli matrix vector $\boldsymbol{\sigma} = (\sigma_x, \sigma_y, \sigma_z)$, with the standard representation in terms of 2×2 matrices obeying an SU(2) Lie algebra. The Pauli matrices are assumed to operate on a spinor basis of spin-up and spin-down electrons denoted by $|\uparrow\rangle$ and $|\uparrow\rangle$, respectively. A set of equations in the valley isospin space completely analogous to those in the spin space results if one defines the SU(2) Pauli-matrix representation for the valley isospin operators $\boldsymbol{\tau} = (\tau_x, \tau_y, \tau_z)$, which operate on the valley isospinor basis with components $|K\rangle$ and $|K\rangle'$. The operators $\boldsymbol{\sigma}$ and $\boldsymbol{\tau}$ may now be used to construct an effective low-energy Hamiltonian having Landau-level and internal spin and valley isospin degrees of freedom.

B. Effective low-energy Hamiltonian

The two largest energy scales for graphene in a strong magnetic field are the Landau-level separation and the

Coulomb energy. At the charge neutral point (Fermi energy for undoped graphene), the LL separation is approximately three times larger than the Coulomb energy, which is in turn considerably larger than any additional terms in the interaction. Therefore a strategy is adopted here of ignoring excitations between Landau levels and projecting onto the $n = 0$ LL. At a quantitative level the Landau level mixing cannot be ignored (see the discussion in Ref. [26]), but such an approximation gives the correct qualitative physics and the effect of excluded Landau levels can be included to some degree by parameter renormalization, which will be sufficient for our purposes.

Within this single Landau level, the Hamiltonian is assumed to be dominated by a long-range Coulomb interaction that is SU(4) symmetric, with shorter-range interactions in spin and valley degrees of freedom (originating in both screened electron-electron interactions and electron-phonon interactions) causing SU(4) symmetry breaking. To implement this, a graphene Hamiltonian projected onto the $n = 0$ Landau level is adopted that was proposed in Ref. [26] and employed further in Ref. [27],

$$H = H_{\rm C} + H_{\rm v} + H_{\rm Z}, \tag{5}$$

where the valley-independent Coulomb interaction $H_{\rm C}$ may be expressed as

$$H_{\rm C} = \frac{1}{2}\sum_{i\neq j}\frac{e^2}{\epsilon|\boldsymbol{r}_i - \boldsymbol{r}_j|}, \tag{6}$$

$H_{\rm v}$ is the short-range, valley-dependent interaction,

$$H_{\rm v} = \frac{1}{2}\sum_{i\neq j}\left[g_z\tau_z^i\tau_z^j + g_\perp\left(\tau_x^i\tau_x^j + \tau_y^i\tau_y^j\right)\right]\delta(\boldsymbol{r}_i - \boldsymbol{r}_j), \tag{7}$$

where the Pauli matrices τ_α operate on the valley isospin and g_z and $g_\perp$ are coupling constants, and the Zeeman energy $H_{\rm Z}$ is given by

$$H_{\rm Z} = -\mu_{\rm B}B\sum_i \sigma_z^i, \tag{8}$$

where $\mu_{\rm B}$ is the Bohr magneton, B is the magnetic field strength, the Pauli matrices σ_α operate on the electronic spin degrees of freedom, and the z direction for the spin space is chosen to be aligned with B.

C. Symmetries of the effective Hamiltonian

Letting $\alpha = (x,y,z)$, $\beta = (x,y)$, and using m_k to label Landau states, the set of 15 operators,

$$\mathcal{S}_\alpha = \sum_{m_k}\sum_{\tau\sigma\sigma'}\langle\sigma'|\sigma_\alpha|\sigma\rangle c^\dagger_{\tau\sigma' m_k}c_{\tau\sigma m_k}, \tag{9a}$$

$$T_\alpha = \sum_{m_k}\sum_{\sigma\tau\tau'}\langle\tau'|\tau_\alpha|\tau\rangle c^\dagger_{\tau'\sigma m_k}c_{\tau\sigma m_k}, \tag{9b}$$

$$N_\alpha = \frac{1}{2}\sum_{m_k}\sum_{\sigma\sigma'\tau}\langle\tau|\tau_z|\tau\rangle\langle\sigma'|\sigma_\alpha|\sigma\rangle c^\dagger_{\tau\sigma' m_k}c_{\tau\sigma m_k}, \tag{9c}$$

$$\Pi_{\alpha\beta} = \frac{1}{2}\sum_{m_k}\sum_{\sigma\sigma'\tau\tau'}\langle\tau'|\tau_\beta|\tau\rangle\langle\sigma'|\sigma_\alpha|\sigma\rangle c^\dagger_{\tau'\sigma' m_k}c_{\tau\sigma m_k}, \tag{9d}$$

is closed under commutation, defining an SU(4) Lie algebra that commutes with the Coulomb interaction $H_{\rm C}$ [26,27]. Thus, if $H_{\rm v}$ and $H_{\rm Z}$ are small compared with $H_{\rm C}$ in Eq. (5), the Hamiltonian will have an approximate SU(4) invariance. The operator $\boldsymbol{\mathcal{S}}$ represents the total spin and the operator $\boldsymbol{T}$ represents the total valley pseudospin. In the $n = 0$ Landau level for graphene there is an equivalence between valley and sublattice degrees of freedom, so $\boldsymbol{N}$ can be viewed as a Néel vector in the $n = 0$ Landau level measuring the difference in spins on the A and B sublattices. The operators $\Pi_{\alpha\beta}$ coupling spin and valley isospin will be discussed further below.

D. Explicit symmetry breaking

The occurrence of SU(4) symmetry and its explicit symmetry-breaking pattern depend on the values of the effective coupling parameters g_z and $g_\perp$. For the lattice spacings found in graphene, each can be estimated to be considerably smaller than the SU(4)-symmetric Coulomb term, so one may expect SU(4) to be broken only weakly by explicit terms in realistic systems. Four basic explicit symmetry-breaking patterns have been identified [26,27].

(1) For arbitrary nonzero values of g_z and $g_\perp$, the symmetry is broken to

$$\mathrm{SU(4)} \supset \mathrm{SU(2)_s}\times\mathrm{U(1)_v} \supset \mathrm{U(1)_s}\times\mathrm{U(1)_v}, \tag{10}$$

where $\mathrm{SU(2)_s}$ is associated with global conservation of spin and $\mathrm{U(1)_s}$ with conservation of its z component, and $\mathrm{U(1)_v}$ is associated with conservation of the T_z component of the valley isospin. (Conservation of T_z implies physically that the difference in electronic densities between the K and K' sites is invariant, which might be expected to be true for low-energy states having minimal scattering between valleys). In the absence of Zeeman splitting, spin is conserved, but only the z component of the valley isospin is conserved. The full Hamiltonian (5) including the Zeeman term conserves only the z components of the spin and valley isospin.

(2) If $g_\perp = 0$ but $g_z \neq 0$, the symmetry is broken to

$$\begin{aligned}\mathrm{SU(4)} &\supset \mathrm{SU(2)_s^K}\times\mathrm{SU(2)_s^{K'}}\times U(1)_{\rm v}\\ &\supset \mathrm{U(1)_s^K}\times\mathrm{U(1)_s^{K'}}\times\mathrm{U(1)_v}.\end{aligned} \tag{11}$$

In the absence of Zeeman splitting, this corresponds to conserving independent spin rotations for the wave function in each valley labeled by K and K', but breaking of the valley isospin to $\mathrm{U(1)_v}$. The full Hamiltonian (5) including the Zeeman term conserves only the z components of the spin in each valley separately, and the z component of the valley isospin.

(3) If $g_{\rm z} = g_\perp \neq 0$, the symmetry is broken to

$$\mathrm{SU(4)} \supset \mathrm{SU(2)_s}\times\mathrm{SU(2)_v} \supset \mathrm{U(1)_s}\times\mathrm{SU(2)_v}, \tag{12}$$

corresponding to full spin and valley isospin rotational symmetry in the absence of Zeeman splitting. The complete Hamiltonian (5) including the Zeeman term conserves the SU(2) isospin symmetry but only the z component of the spin.

(4) If $g_\perp = -g_z \neq 0$, the Hamiltonian commutes with $\Pi_{\alpha\beta}$, $\boldsymbol{\mathcal{S}}$, and T_z, and these ten operators generate the Lie group SO(5), so [27]

$$\mathrm{SU(4)} \supset \mathrm{SO(5)} \supset \mathrm{U(1)_s}\times\mathrm{SU(2)_z}, \tag{13}$$

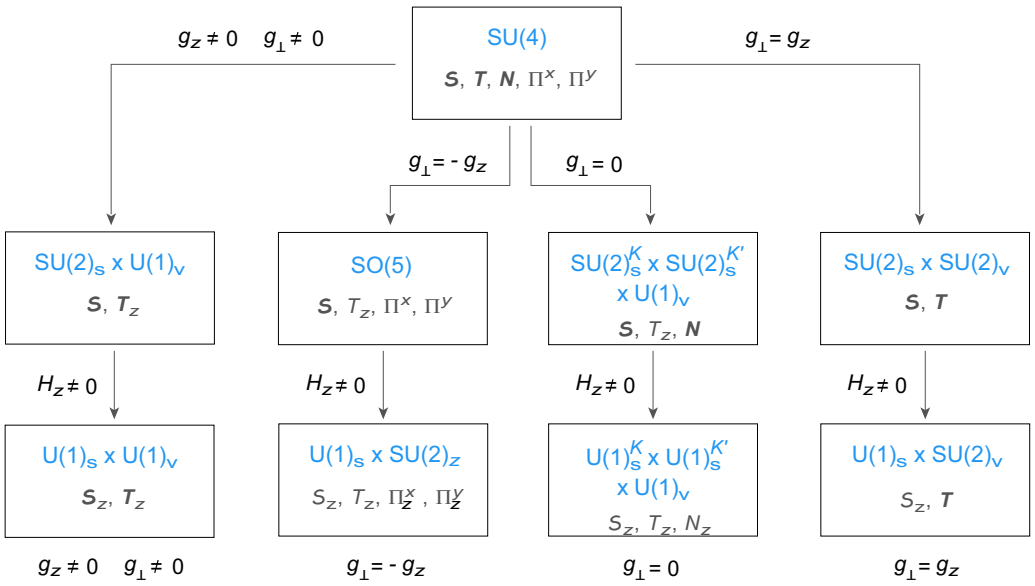

FIG. 3. Explicit symmetry-breaking structure for SU(4) quantum Hall ferromagnetism described by the Hamiltonian (5).

where the $SU(2)_z$ symmetry is generated by $(T_z, \Pi_{zx}, \Pi_{zy})$. Thus, in the absence of Zeeman splitting, the system exhibits an SO(5) symmetry involving both spin and valley isospin. The full Hamiltonian (5) including the Zeeman term conserves the z component of spin and the $SU(2)_z$ symmetry. The SO(5) subgroup plays the role of a transitional symmetry connecting the Néel-like states associated with N_α and the states associated with valley degrees of freedom T_x and T_y.

The subgroup structure for these four patterns of explicit SU(4) symmetry breaking is illustrated in Fig. 3. These symmetries and explicitly broken symmetries have proven extremely useful in understanding the states of graphene in a strong magnetic field [26,27] .

VII. FERMION DYNAMICAL SYMMETRIES

Let us now consider using symmetries in an even more powerful way than that discussed in the preceding section. Specifically, let us attempt to describe the quantum Hall ferromagnetic behavior of graphene using *fermion dynamical symmetries* of an effective Hamiltonian operating in a highly truncated collective subspace. This has the potential to prescribe dynamics as well as taxonomy and conservation laws, within a many-body model having analytical solutions that illuminate the physics of quantum Hall states in graphene.

As noted in the Introduction and elaborated in Refs. [16–20], application of these methods requires identifying on physical grounds a highest symmetry, constructing associated group generators expressed in terms of second-quantized fermionic operators, identifying subgroup chains of physical relevance and the invariant Casimir operators associated with those subgroup chains, and specifying a convenient description of the basis wave functions in the Hilbert subspace that is selected by the dynamical symmetry truncation. In addition, for the specific problem being considered here it is important to elucidate how the description of graphene in a strong magnetic field in the dynamical symmetry formalism is related to prior SU(4) quantum Hall ferromagnet descriptions of the same problem. These will be developed in Secs. VII–XIV, and used beginning in Sec. XV to find dynamical symmetry solutions for the graphene problem.

A. Symmetry generators

For clarity of discussion, a valence space will be assumed corresponding to a single Landau level. To avoid cluttered notation, the index n labeling the Landau level is suppressed and the fermion creation operator $c^\dagger_{\tau\sigma m_k}$ and the corresponding hermitian conjugate $c_{\tau\sigma m_k}$ are introduced. The index τ takes one of two values ($\pm$) labeling the valley isospin projections corresponding to valleys K or K', the electron spin polarization σ takes one of two values ($\uparrow\downarrow$) labeling spin up or spin down, and m_k is a quantum number distinguishing degenerate states within a given Landau level (typically, an angular momentum in symmetric gauge or a linear momentum in Landau gauge). By virtue of the anticommutation of the fermionic operators, the $c^\dagger_\alpha$ create a fermion in the state labeled by α, the c_α annihilate a fermion in the same state, and $n_\alpha = c^\dagger_\alpha c_\alpha$ counts the number of fermions in the state labeled by α.

The four states representing possible combinations of τ and σ are displayed in Table I, and correspond physically to the four possible combinations of the electron being in either the K or K' valley with either spin up or spin down [see Fig. 2(b)]. For brevity the label $a = 1,2,3,4$ displayed in the last column of the table will often be used to distinguish these states. The

TABLE I. Quantum numbers.

Valley	τ	σ	m_i	a
K	$+$	$\uparrow$	$+\frac{3}{2}$	1
K	$+$	$\downarrow$	$+\frac{1}{2}$	2
K'	$-$	$\uparrow$	$-\frac{1}{2}$	3
K'	$-$	$\downarrow$	$-\frac{3}{2}$	4

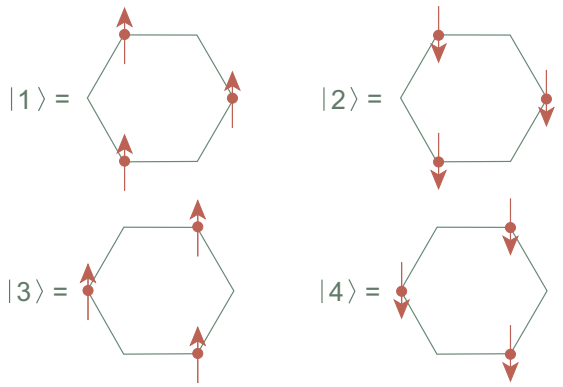

FIG. 4. The four isospin-spin basis vectors $|a\rangle$ of Table I.

four basis states labeled by a are illustrated graphically in Fig. 4.

Table I also displays a unique mapping of these four states to a label m_i that takes the four possible projection quantum numbers $\{\pm\frac{1}{2}, \pm\frac{3}{2}\}$ of a fictitious angular momentum $i = \frac{3}{2}$; the motivation for this mapping will become apparent later.

Let us now introduce an operator $A^\dagger_{ab}$ that creates a pair of electrons, one in the $a = (\tau_1,\sigma_1)$ level and one in the $b = (\tau_2,\sigma_2)$ level, with the total m_k of each pair coupled to zero term by term,

$$A^\dagger_{ab} = \sum_{m_k} c^\dagger_{am_k} c^\dagger_{b-m_k}, \tag{14}$$

and its hermitian conjugate A_{ab}, which annihilates a corresponding electron pair. Each index a or b ranges over four values, implying 16 components in Eq. (14). However, the pair wave function must satisfy the Pauli principle which, upon expanding the indices a and b using Table I, eliminates the four diagonal ($a = b$) possibilities. Furthermore, because of the antisymmetry requirement the pair creation operators are constrained by $A^\dagger_{ab} = -A^\dagger_{ba}$, implying that only half of the remaining 12 operators $A^\dagger$ are independent. Thus Eq. (14) defines six independent operators $A^\dagger$, with six independent hermitian conjugates A. Let us introduce in addition to these pairing operators the 16 particle-hole operators B_{ab} through

$$B_{ab} = \sum_{m_k} c^\dagger_{am_k} c_{bm_k} - \frac{1}{4}\delta_{ab}\Omega, \tag{15}$$

where δ_{ab} is the Kronecker delta and Ω is the total degeneracy of the single Landau level [see Eq. (22)]. The commutators for the 28 operators A, $A^\dagger$, and B are found to be [28]

$$[A_{ab}, A^\dagger_{cd}] = -B_{db}\delta_{ac} - B_{ca}\delta_{bd} + B_{cb}\delta_{ad} + B_{da}\delta_{bc}, \tag{16a}$$
$$[B_{ab}, B_{cd}] = \delta_{bc}B_{ad} - \delta_{ad}B_{cb}, \tag{16b}$$
$$[B_{ab}, A^\dagger_{cd}] = \delta_{bc}A^\dagger_{ad} + \delta_{bd}A^\dagger_{ca}, \tag{16c}$$
$$[B_{ab}, A_{cd}] = -\delta_{ac}A_{bd} - \delta_{ad}A_{cb}, \tag{16d}$$

which is isomorphic to an SO(8) Lie algebra. Thus the 28 members of the operator set $(A, A^\dagger, B)$ exhibit SO(8) symmetry under commutation.

B. Relationship with standard graphene SU(4) symmetry

The SU(4) generators (9) may be expressed in terms of the operators (15) by utilizing the equivalences in Table I to expand the indices for B_{ab} from Eq. (15). As an example, consider the spin operator $\mathcal{S}_y$. From Eq. (9a),

$$\begin{aligned}\mathcal{S}_y &= \sum_{m_k}\sum_{\tau\sigma\sigma'}\langle\sigma'|\sigma_y|\sigma\rangle c^\dagger_{\tau\sigma' m_k} c_{\tau\sigma m_k}\\ &= \sum_{m_k}\big(-ic^\dagger_{+\uparrow m_k}c_{+\downarrow m_k} + ic^\dagger_{+\downarrow m_k}c_{+\uparrow m_k}\\ &\quad - ic^\dagger_{-\uparrow m_k}c_{-\downarrow m_k} + ic^\dagger_{-\downarrow m_k}c_{-\uparrow m_k}\big)\\ &= -iB_{12} + iB_{21} - iB_{34} + iB_{43}.\end{aligned}$$

By such methods one finds that the spin operators (9a) may be expressed in terms of the B_{ab} generators of SO(8) as

$$\mathcal{S}_x = B_{12} + B_{21} + B_{34} + B_{43}, \tag{17a}$$
$$\mathcal{S}_y = -i(B_{12} - B_{21} + B_{34} - B_{43}), \tag{17b}$$
$$\mathcal{S}_z = B_{11} - B_{22} + B_{33} - B_{44}, \tag{17c}$$

the valley isospin operators (9b) as

$$T_x = B_{13} + B_{31} + B_{24} + B_{42}, \tag{18a}$$
$$T_y = -i(B_{13} - B_{31} + B_{24} - B_{42}), \tag{18b}$$
$$T_z = B_{11} + B_{22} - B_{33} - B_{44}, \tag{18c}$$

The Néel vector of Eq. (9c) as

$$N_x = \frac{1}{2}(B_{12} + B_{21} - B_{34} - B_{43}), \tag{19a}$$
$$N_y = -\frac{i}{2}(B_{12} - B_{21} - B_{34} + B_{43}), \tag{19b}$$
$$N_z = \frac{1}{2}(B_{11} - B_{22} - B_{33} + B_{44}), \tag{19c}$$

and the operators $\Pi_{\alpha\beta}$ of Eq. (9d) as

$$\Pi_{xx} = \frac{1}{2}(B_{14} + B_{41} + B_{23} + B_{32}), \tag{20a}$$
$$\Pi_{yx} = -\frac{i}{2}(B_{23} - B_{32} + B_{41} - B_{14}), \tag{20b}$$
$$\Pi_{zx} = \frac{1}{2}(B_{13} + B_{31} - B_{24} - B_{42}), \tag{20c}$$
$$\Pi_{xy} = -\frac{i}{2}(B_{32} - B_{23} + B_{41} - B_{14}), \tag{20d}$$
$$\Pi_{yy} = -\frac{1}{2}(B_{41} + B_{14} - B_{23} - B_{32}), \tag{20e}$$
$$\Pi_{zy} = -\frac{i}{2}(B_{31} - B_{13} - B_{42} + B_{24}). \tag{20f}$$

The inverse transformations expressing the B_{ab} in terms of the $\{\mathcal{S}_\alpha, T_\alpha, N_\alpha, \Pi_{\alpha x}, \Pi_{\alpha y}\}$ are given in Appendix. Hence the SU(4) algebra generated by the operators in Eq. (9) is a subalgebra of the SO(8) algebra, with its generators corresponding to particular linear combinations of the subset of SO(8) generators defined by the particle-hole operators B_{ab} in Eq. (15).

TABLE II. Pair degeneracies Ω for magnetic field strengths B.

Domain size	$B = 2$ T	$B = 10$ T	$B = 50$ T
$5\ \mu\text{m} \times 5\ \mu\text{m}$	24,150	120,750	603,750
$10\ \mu\text{m} \times 10\ \mu\text{m}$	96,660	483,000	2.145×10^6

VIII. PAIR REPRESENTATIONS

Pairs of fermions often afford a convenient basis for discussing collective states, so let us consider some possible configurations involving pairs of electrons in graphene.

A. Degeneracies and level filling

Consider the degeneracies of undoped graphene placed in a strong magnetic field, confining the discussion to the case of a single Landau level for simplicity. The single-particle states within the Landau level will be assumed labeled by the quantum numbers (n,m_k), where n is the principle quantum number indicating the Landau level and m_k is a quantum number distinguishing the degenerate states within the Landau level. In the absence of spin and valley degrees of freedom, the states (n,m_k) of the Landau level are assumed to hold a maximum of $2\Omega_k$ electrons. From the solution of the Dirac equation in a magnetic field

$$2\Omega_k = \frac{BS}{(h/e)}, \tag{21}$$

where B is the strength of the magnetic field, S is the area of the two-dimensional sample and $h/e = 4.136 \times 10^{-15}$ Wb defines the magnetic flux quantum. But graphene has in addition four internal degrees of freedom associated with the $|\text{spin}\rangle \otimes |\text{isospin}\rangle$ space. Thus there are four copies of each Landau level in graphene and the total electron degeneracy 2Ω is given by

$$2\Omega = 4(2\Omega_k) = \frac{4BS}{(h/e)}. \tag{22}$$

Some pair degeneracies calculated from Eq. (22) as a function of domain size and magnetic field strength are displayed in Table II, where it is assumed that the collective wave function is delocalized over the entire domain size.

The *fractional occupation* f of the single Landau level [not to be confused with the filling factor ν given in Eqs. (2) and (25)] may be defined as

$$f \equiv \frac{n}{2\Omega} = \frac{N}{\Omega}, \tag{23}$$

where n is the number of electrons and $N = \frac{1}{2}n$ is the number of electron pairs. For half-filling of the $n = 0$ Landau level located at the Fermi surface (corresponding to the ground state of undoped graphene) the electron number n_{gs} is then

$$n_{\text{gs}} = \Omega = \frac{2BS}{(h/e)}. \tag{24}$$

These degeneracies and occupation numbers are just the standard results for relativistic Landau levels in a 2D electron gas subject to a strong perpendicular magnetic field, but modified by the graphene spin and valley degeneracies.

Graphene exhibits both integral and fractional quantum Hall effects but the filling factors are anomalous relative to those for standard quantum Hall effects in semiconductor heterostructures. This is because of (1) the fourfold degeneracy associated with the spin and valley degrees of freedom and (2) the nature of the Dirac solution, illustrated in Fig. 2, for which the negative-energy solutions may be interpreted as electron holes, the positive-energy solutions as electrons, and the $n = 0$ level is unique, being half-filled in the neutral ground state.

Because of the particle-hole symmetry, the charge carriers change sign near the Dirac points and the Hall conductivity vanishes at charge neutrality (the electron number density tends to zero at a Dirac point). For this reason, the filling factor for graphene must be defined *relative to the charge-neutral state.* At charge neutrality the $n = 0$ Landau level is half-filled and when the $n = 0$ LL is completely full the filling factor is $4 \times \frac{1}{2} = 2$, from Eq. (4). The quantum Hall filling factor ν may be related to the Landau level fractional occupation f employed in the present formalism by

$$\nu = 4\left(f - \frac{1}{2}\right) = 4\left(\frac{n}{2\Omega} - \frac{1}{2}\right). \tag{25}$$

Therefore half-filling of the $n = 0$ Landau level corresponds to a fractional occupation $f = \frac{1}{2}$ but to a filling factor $\nu = 0$, $\nu = -2$ corresponds to $f = 0$ (completely empty), $\nu = -1$ corresponds to $f = \frac{1}{4}$ filling, $\nu = +1$ corresponds to $f = \frac{3}{4}$ filling, and $\nu = +2$ corresponds to $f = 1$ (completely full).

B. Many-pair states

Consider the states created by repeated application of the pair creation operator $A^\dagger_{ab}$ defined by Eq. (14) to the pair vacuum. It is useful to classify states according to a senioritylike quantum number u defined to be the number of particles in the system not coupled to one of the pairs defined in Eq. (14). The $u = 0$ subspace will be of particular interest since it will contain states of maximal collectivity with respect to the pairs (14). An N-pair state in the $u = 0$ subspace is given by

$$(A^\dagger_{12})^{N_{12}}(A^\dagger_{13})^{N_{13}}(A^\dagger_{14})^{N_{14}}(A^\dagger_{23})^{N_{23}}(A^\dagger_{24})^{N_{24}}(A^\dagger_{34})^{N_{34}}\,|0\rangle, \tag{26}$$

where the total pair number N is

$$N = \tfrac{1}{2}n = N_{12} + N_{13} + N_{14} + N_{23} + N_{24} + N_{34}, \tag{27}$$

with n giving the total number of electrons and N_{ab} giving the number of electron pairs created by $A^\dagger_{ab}$ operating on the vacuum state. For our discussion here it will always be assumed that one is dealing with $u = 0$ states, corresponding physically to no broken pairs.

C. States in SO(8) ⊃ SU(4) irreducible representations

From Eq. (16), the 16 operators B_{ab} are closed under commutation and form a U(4) ⊃ U(1) × SU(4) subalgebra of the SO(8) algebra (16). Let us now investigate the irreducible representations (irreps) that are associated with the SO(8) ⊃ SU(4) subgroup chain in the $u = 0$ representations.

1. The highest-weight state

For $u = 0$ at half-filling, the number of pairs is $N = \frac{1}{2}\Omega = 2k + 1$ and the highest-weight U(4) representation is given by $(\frac{\Omega}{2},\frac{\Omega}{2},0,0)$. Let us define a highest-weight (HW) state in the $u = 0$ space, and choose it to correspond to the pair state with maximal value of m_i from Table I, which results from placing one electron in the $a = 1$ state and one electron in the $a = 2$ state. Thus, for $N = 2k + 1$ pairs, the highest weight state is given by

$$|\mathrm{HW}\rangle = \frac{1}{(2k+1)!}(A_{12}^{\dagger})^{2k+1}|0\rangle = \frac{1}{(2k+1)!}\left(\sum_{m_k} c_{1m_k}^{\dagger} c_{2,-m_k}^{\dagger}\right)^{2k+1}|0\rangle, \quad (28)$$

where the sum runs over the $2k + 1$ states in the Landau level labeled by the $m_k = (-k, -k+1, \ldots, k-1, k)$ quantum number. The other states of the irreducible representation may then be created by the Cartan-Dynkin algorithm, which consists of using raising and lowering operators in the weight space to construct successively all the other states beginning with the highest weight state [29].

The state in Eq. (28) appears to have a quite complex form, involving a sum with number of terms equal to the pair degeneracy of the Landau level raised to a power equal to the pair degeneracy (with the pair degeneracy typically a very large number). However, the actual structure of this state is considerably simpler than Eq. (28) would suggest because of the Pauli principle. As an illustrative example of this assertion, let us construct explicitly the highest-weight state for the case $k = 1$, corresponding to $2k + 1 = 3$ pairs in a single Landau level. Writing the sum over $m_k = (-1,0,+1)$ in Eq. (28) out term by term gives

$$|\mathrm{HW}\rangle = \frac{1}{3!}(c_{1,-1}^{\dagger}c_{21}^{\dagger} + c_{10}^{\dagger}c_{20}^{\dagger} + c_{11}^{\dagger}c_{2,-1}^{\dagger})^3|0\rangle = c_{10}^{\dagger}\,c_{20}^{\dagger}\,c_{11}^{\dagger}\,c_{21}^{\dagger}\,c_{1,-1}^{\dagger}\,c_{2,-1}^{\dagger}\,|0\rangle = \prod_{m_k=-k}^{m_k=+k} c_{1m_k}^{\dagger}c_{2m_k}^{\dagger}|0\rangle,$$

where in raising the sum of operators inside the parentheses to the $2k + 1 = 3$ power, all products containing two or more creation operators with the same index vanish because of the Pauli principle. Similar considerations apply for arbitrary values of k and in general the highest-weight state is given by

$$|\mathrm{HW}\rangle = \frac{1}{N!}(A_{12}^{\dagger})^N|0\rangle = \frac{1}{N!}\left(\sum_{m_k} c_{1m_k}^{\dagger}c_{2-m_k}^{\dagger}\right)^N|0\rangle = \prod_{m_k=-k}^{m_k=+k} c_{1m_k}^{\dagger}c_{2m_k}^{\dagger}|0\rangle, \quad (29)$$

where the simplification in the last step is a consequence of the antisymmetry of the fermion creation operators (the Pauli principle). Thus the highest-weight state is a product state of pairs, one pair for each of the $N = 2k + 1$ levels labeled by m_k in the Landau level.

2. Other SO(8) ⊃ SU(4) states

By the Cartan-Dynkin algorithm, other states in the $u = 0$ subspace can be constructed by applying successively to the highest-weight state appropriate lowering and raising operators. These will be functions of the generators B_{ab}, so for an arbitrary state $|\psi\rangle$ in the weight space one has schematically $|\psi\rangle = F(B_{ab})|\mathrm{HW}\rangle$, where the function $F(B_{ab})$ is specified by the Cartan-Dynkin procedure. As an example, consider the action of the valley isospin lowering operator T_- on the highest-weight state. From Eqs. (18) and (15),

$$T_- \equiv \frac{1}{2}(T_x - iT_y) = \sum_{m_k}\left(c_{K'\uparrow m_k}^{\dagger}c_{K\uparrow m_k} + c_{K'\downarrow m_k}^{\dagger}c_{K'\downarrow m_k}\right).$$

Thus the state $|\psi\rangle$ created by applying T_- to $|\mathrm{HW}\rangle$ is

$$|\psi\rangle = \prod_{m_k}\left[\sum_{n_k}\left(c_{K'\uparrow n_k}^{\dagger}c_{K\uparrow n_k} + c_{K'\downarrow n_k}^{\dagger}c_{K'\downarrow n_k}\right)\right]c_{K\uparrow m_k}^{\dagger}c_{K\downarrow m_k}^{\dagger}|0\rangle = \prod_{m_k}\left(c_{3m_k}^{\dagger}c_{2m_k}^{\dagger} + c_{4m_k}^{\dagger}c_{1m_k}^{\dagger}\right)|0\rangle, \quad (30)$$

where the simplifications are because the only terms that survive correspond to those where an annihilation operator in a factor inside the square brackets is exactly balanced by a creation operator from the factor outside the square brackets. Likewise, the other states of the $u = 0$ representation can be constructed by using successive applications of raising and lowering operators fashioned from the generators defined in in Eqs. (17)–(20).

D. Equivalence of pair and product wave functions

From the preceding, for $N = \frac{1}{2}\Omega$ states may be written as

$$|\psi\rangle = F(B_{ab})|\mathrm{HW}\rangle = \prod_{m_k}\left[\sum_{\tau\sigma\tau'\sigma'}\Phi^{*}_{\tau\sigma\tau'\sigma'}c_{\tau\sigma m_k}^{\dagger}c_{\tau'\sigma' m_k}^{\dagger}\right]|0\rangle, \quad (31)$$

where τ,τ' denote valley isospin projection quantum numbers and σ,σ' denote spin projection quantum numbers. This is the same form as the most general collective pair state used by Kharitonov [26] in his classification of possible broken symmetry states for the $n = 0$ Landau level in graphene. Thus, for undoped graphene, the general pairing wave function (26) characteristic of the SO(8) ⊃ SU(4) dynamical symmetry is in fact *equivalent to the product form (31)* employed in standard discussion of quantum Hall ferromagnetism, for which the summations are over the internal (τ,σ) rather than Landau (m_k) degrees of freedom. The equivalence of Eqs. (31) and (26), despite their superficially very different forms, is a fundamental consequence of the Pauli principle acting in the collective fermionic pair subspace, which greatly restricts allowed pair configurations.

IX. BEYOND QUANTUM HALL FERROMAGNETISM

The preceding discussion has established that the fermion dynamical symmetry method applied to undoped graphene in a strong magnetic field has one dynamical symmetry chain SO(8) ⊃ SU(4) that recovers exactly SU(4)-symmetric

quantum Hall ferromagnetism. Since the B_{ab} operators introduced in Eq. (15) form an SU(4) subgroup of SO(8) that is in one-to-one correspondence with the operators used to formulate the effective low-energy Hamiltonian (5), Sec. VII implies that all of the physics associated with this effective Hamiltonian that has been discussed in the prior literature (see Refs. [26,27] and references cited therein) is implicit in the present formalism.

Furthermore, the discussion of Sec. VIII shows that the pair basis (26) of the truncated collective subspace for the SO(8) fermion dynamical symmetry is in fact identical to the most general wave function (31) that has been proposed [26] for collective states breaking the SU(4) symmetry, despite its superficially very different form. Thus the Hilbert-space truncation implied by the collectively paired SO(8) subspace (26) recovers the understanding in the existing literature of the classes of states to be expected from spontaneous breaking of the SU(4) symmetry by valley-dependent correlations.

However, the existing discussions of these collective states in terms of broken SU(4) symmetry have been largely qualitative, and have turned to numerical simulations to discuss the actual structure and energy of the states. It will now be demonstrated that the present formalism is capable not only of classifying, but also of addressing the quantitative nature of those collective states *in analytical fashion.* This is simpler than numerical simulation, easier to visualize conceptually, and avoids errors associated with use of small bases in numerical simulations done to date. Furthermore, it will be shown that the SO(8) highest symmetry implies subgroup chains in addition to SO(8) $\supset$ SU(4) that are associated with spontaneous breaking of the symmetry by correlations and have not been discussed in the previous literature and that may play a role in graphene.

Let us begin that discussion by first transforming to a more convenient representation of the SO(8) generators. This new representation will be physically equivalent to the original representation, but will offer some advantages in interpretation, and will expose an unexpected relationship between graphene physics and that of a very different field, nuclear structure physics.

X. COUPLED REPRESENTATIONS

For the pair creation operators defined in Eq. (14), each electron creation operator $c^\dagger$ carries both spin and valley isospin; hence the products $c^\dagger c^\dagger$ correspond to a Clebsch-Gordan series representing sums of terms having different values of total spin and total isospin. Likewise, in the particle-hole operators of Eq. (15) each creation operator $c^\dagger$ and annihilation operator c carries spin and isospin, so the product $c^\dagger c$ in Eq. (15) represents a superposition of states carrying different total spin and total valley isospin. These representations with indefinite spin and isospin will be termed *uncoupled representations.*

On physical grounds, the spin is expected to be conserved (if the Zeeman term in the Hamiltonian is neglected) and the valley isospin is expected to be approximately conserved for low-energy excitations. Thus it is desirable to use the uncoupled representation of the pairing and particle-hole operators to construct new *coupled representations* that have good total spin and good total valley isospin quantum numbers for bilinear operators.

A. Coupled representation for pairing operators

Using standard angular momentum coupling theory [30], an electron pair creation operator coupled to good spin and valley isospin may be defined by

$$A^{\dagger ST}_{M_S M_T} \equiv \sum_{m_1 m_2 n_1 n_2} C^{SM_S}_{\frac{1}{2}m_1\frac{1}{2}m_2} C^{TM_T}_{\frac{1}{2}n_1\frac{1}{2}n_2} c^\dagger_{m_1 n_1 m_k} c^\dagger_{m_2 n_2 - m_k}, \quad (32)$$

where S is the total spin of the pair with M_S its projection, T is the total valley isospin of the pair with M_T its projection, and $C^{JM}_{j_1 m_1 j_2 m_2}$ are Clebsch-Gordan coefficients for the angular momentum sum $\boldsymbol{j}_1 + \boldsymbol{j}_2 = \boldsymbol{j}$ that couple the pair to good total spin or total valley isospin. Antisymmetry implies that the pair wave function can have only $S = 1, T = 0$; or $S = 0, T = 1$ (spin-triplet, isospin-singlet; or spin-singlet, isospin-triplet pairs). Explicitly the possibilities are

$$\begin{aligned} A^{\dagger 10}_{00} &= A^\dagger_{14} - A^\dagger_{23}, \quad A^{\dagger 10}_{10} = \sqrt{2} A^\dagger_{12}, \quad A^{\dagger 10}_{-10} = \sqrt{2} A^\dagger_{34} \\ A^{\dagger 01}_{00} &= A^\dagger_{14} + A^\dagger_{23}, \quad A^{\dagger 01}_{01} = \sqrt{2} A^\dagger_{13}, \quad A^{\dagger 01}_{0-1} = \sqrt{2} A^\dagger_{24}, \end{aligned} \quad (33)$$

with the Hermitian conjugates of Eq. (33) giving the six corresponding pair annihilation operators in coupled representation. It is useful to define an alternative set of six coupled pairing operators $S^\dagger$ and $D^\dagger_\mu (\mu = 0, \pm 1, \pm 2)$ according to

$$\begin{aligned} S^\dagger &= \frac{1}{\sqrt{2}} A^{\dagger 10}_{00} = \frac{1}{\sqrt{2}} (A^\dagger_{14} - A^\dagger_{23}), \\ D^\dagger_0 &= \frac{1}{\sqrt{2}} A^{\dagger 01}_{00} = \frac{1}{\sqrt{2}} (A^\dagger_{14} + A^\dagger_{23}), \\ D^\dagger_1 &= \frac{1}{\sqrt{2}} A^{\dagger 01}_{01} = A^\dagger_{13}, \quad D^\dagger_{-1} = \frac{1}{\sqrt{2}} A^{\dagger 01}_{0-1} = A^\dagger_{24}, \\ D^\dagger_2 &= \frac{1}{\sqrt{2}} A^{\dagger 10}_{10} = A^\dagger_{12}, \quad D^\dagger_{-2} = \frac{1}{\sqrt{2}} A^{\dagger 10}_{-10} = A^\dagger_{34}, \end{aligned} \quad (34)$$

and the six corresponding hermitian conjugates S and D_μ. The physical meaning of these pairs may be deduced by constructing the corresponding electronic configurations. As an example, consider $D^\dagger_2$. From Eqs. (34) and (14),

$$D^\dagger_2 = \frac{1}{\sqrt{2}} A^{\dagger 10}_{10} = A^\dagger_{12} = \sum_{m_k} c^\dagger_{1 m_k} c^\dagger_{2 - m_k} = \sum_{m_k} c^\dagger_{K \uparrow m_k} c^\dagger_{K \downarrow - m_k},$$

where in the last step the correspondence between the index $a = 1,2,3,4$ and the valley (K or K') and spin ($\uparrow\downarrow$) labels in Table I has been invoked. This implies that $D^\dagger_2|0\rangle$ creates a state with one spin-up and one spin-down electron on each equivalent site K in the Brillouin zone, as illustrated schematically in Fig. 5.

This is a component of a lattice-scale charge density wave, since the charge differs by two electronic units between adjacent sites. Likewise, one finds that $D^\dagger_{-2}|0\rangle$ creates a charge density wave as in Fig. 5, but with the spin-singlet pairs on the K' sites. The pair configurations produced by all generators of Eq. (34) operating on the pair vacuum $|0\rangle$ are summarized in Fig. 6.

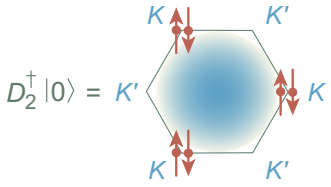

FIG. 5. The action of the pair creation operator $D_2^\dagger$ on the vacuum state is to create a charge density wave with a spin-singlet pair on each site K and no electrons on the K' sites.

Also shown are the configurations generated by the linear combinations

$$|Q_\pm\rangle = Q_\pm^\dagger|0\rangle \equiv \tfrac{1}{2}(S^\dagger \pm D_0^\dagger)|0\rangle = \tfrac{1}{2}(|S\rangle \pm |D_0\rangle), \quad (35)$$

which will be useful in later discussion.

Kharitonov has given a general classification of low-lying collective modes for the $n = 0$ Landau level of graphene in terms of collective pairs [26]. The collective pairs created by the SO(8) pair generators in Fig. 6 are similar physically to the pairs identified by Kharitonov, as will now be described.

(1) The configuration generated by $S^\dagger|0\rangle$ is proportional to the difference of two terms, each with alternating spin up and spin down on adjacent sites, implying that all spins on the A sublattice (identified with valley K) point in one direction and all spins on the B sublattice (identified with valley K') point in the opposite direction. Each term corresponds to a spin density wave (AF order), with a Néel vector defined by the difference in total spins on the two sublattices serving as an order parameter, but because of the difference of the two terms the net AF order for this configuration is zero (see Sec. XIV A and Table III).

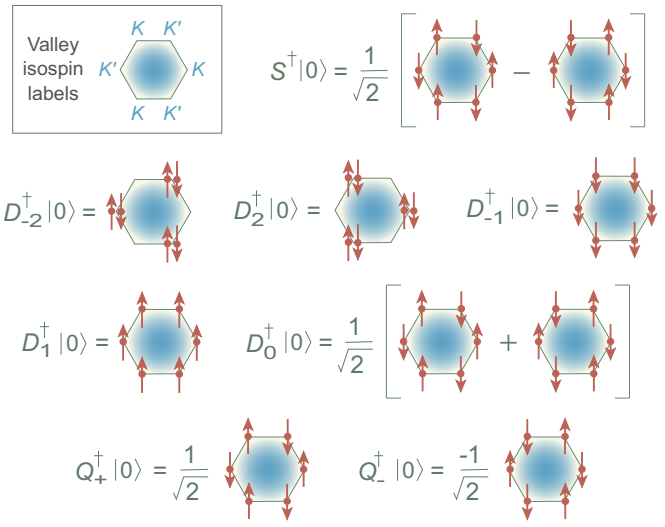

FIG. 6. Configurations created by the $S^\dagger$ and $D_\mu^\dagger$ pair creation operators of Eq. (34), and for the linear combinations $Q_\pm$ of Eq. (35), operating on the pair vacuum $|0\rangle$. The upper left box illustrates the valley isospin labeling. A total of six valence electrons as assumed to be distributed on sites in the Brillouin zone. In each pair configuration, location of the dots (K or K' site) indicates the valley isospin, spin-up electrons are indicated by up arrows, and spin-down electrons are indicated by down arrows.

TABLE III. Order parameters for states in Fig. 6.

State	$\langle S_z\rangle$	$\langle T_z\rangle$	$\langle N_z\rangle$
$\|S\rangle = S^\dagger\|0\rangle$	0	0	0
$\|D_{-2}\rangle = D_{-2}^\dagger\|0\rangle$	0	−1	0
$\|D_2\rangle = D_2^\dagger\|0\rangle$	0	1	0
$\|D_{-1}\rangle = D_{-1}^\dagger\|0\rangle$	−1	0	0
$\|D_1\rangle = D_1^\dagger\|0\rangle$	1	0	0
$\|D_0\rangle = D_0^\dagger\|0\rangle$	0	0	0
$\|Q_+\rangle = \frac{1}{2}(\|S\rangle + \|D_0\rangle)$	0	0	1
$\|Q_-\rangle = \frac{1}{2}(\|S\rangle - \|D_0\rangle)$	0	0	−1

(2) The configurations generated by $D_{\pm2}^\dagger|0\rangle$ correspond to spin-singlet charge density waves, with alternating charges of two and zero units on adjacent sites. An appropriate order parameter is the difference in charge between the A and B sublattices.

(3) The configurations generated by $D_{\pm1}^\dagger|0\rangle$ have one spin on each site, all pointing in the same direction; this is a ferromagnetic state, with the net spin as an order parameter.

(4) The configuration generated by $D_0^\dagger|0\rangle$ is the same as that generated by $S^\dagger|0\rangle$, except for a positive sign for the second term. This also implies alternating spins on adjacent sites and AF order for each term, but the total AF order vanishes because of the contribution of the two terms.

(5) The configurations corresponding to $Q_\pm^\dagger|0\rangle$ are states with AF order characterized by the difference in spins on the two sublattices labeled by K and K'.

Therefore it may be concluded that the pairs carrying good spin and valley isospin in Eq. (34) represent physical degrees of freedom already discussed in the literature as candidate collective modes representing spontaneous breaking of the SU(4) graphene symmetry by interactions in a single partially filled Landau level.

B. Coupled representation for particle-hole operators

It is desirable to express the particle-hole generators of Eq. (15) in coupled representation. Let us begin by introducing a set of operators

$$P_\mu^r = \sum_{m_j m_l} (-1)^{\frac{3}{2}+m_\ell} C^{r\,\mu}_{\frac{3}{2}m_j\,\frac{3}{2}m_\ell} B_{m_j - m_\ell}, \quad (36)$$

with the definition

$$B_{m_j-m_\ell} \equiv \sum_{m_k} c^\dagger_{m_j m_k} c_{-m_\ell m_k} - \frac{1}{4}\delta_{m_j-m_\ell}\Omega, \quad (37)$$

where m_j and m_ℓ take the values of the fictitious angular momentum projection m_i in Table I, providing a labeling equivalent to that of a and b in B_{ab}, with m_j or m_ℓ values $\{\frac{3}{2},\frac{1}{2},-\frac{1}{2},-\frac{3}{2}\}$ mapping to a or b values $\{1,2,3,4\}$, respectively. For example, from Table I, $B_{ab} = B_{12}$ and $B_{m_j m_\ell} = B_{3/2,1/2}$ label the same quantity, which is defined in Eq. (15). From the standard selection rules for coupling of angular momentum in Eq. (36), the index r can take the values $r = 0,1,2,3$, with $2r+1$ projections μ for each possibility, which gives a total of 16 operators P_μ^r. By inserting the explicit values of the

Clebsch-Gordan coefficients the 16 independent P^r_μ may be evaluated in terms of the B_{ab} to give

$$
\begin{aligned}
P^0_0 &= \frac{1}{2}(B_{11}+B_{22}+B_{33}+B_{44}) \\
&= \frac{1}{2}(n_1+n_2+n_3+n_4-\Omega) = \frac{1}{2}(n-\Omega), \\
P^1_0 &= \sqrt{\frac{9}{20}}(B_{11}-B_{44})+\sqrt{\frac{1}{20}}(B_{22}-B_{33}) \\
&= \sqrt{\frac{9}{20}}(n_1-n_4)+\sqrt{\frac{1}{20}}(n_2-n_3), \\
P^1_1 &= -\sqrt{\frac{3}{10}}\,B_{12}-\sqrt{\frac{4}{10}}\,B_{23}-\sqrt{\frac{3}{10}}\,B_{34}, \\
P^1_{-1} &= \sqrt{\frac{3}{10}}\,B_{21}+\sqrt{\frac{4}{10}}\,B_{32}+\sqrt{\frac{3}{10}}\,B_{43}, \\
P^2_0 &= \frac{1}{2}(B_{11}-B_{22}+B_{44}-B_{33}) \\
&= \frac{1}{2}(n_1-n_2+n_4-n_3), \\
P^2_1 &= \frac{1}{\sqrt{2}}(B_{34}-B_{12}), \quad P^2_{-1} = \frac{1}{\sqrt{2}}(B_{21}-B_{43}), \\
P^2_2 &= -\frac{1}{\sqrt{2}}(B_{13}+B_{24}), \quad P^2_{-2} = -\frac{1}{\sqrt{2}}(B_{31}+B_{42}), \\
P^3_0 &= \sqrt{\frac{1}{20}}(B_{11}-B_{44})+\sqrt{\frac{9}{20}}(B_{33}-B_{22}) \\
&= \sqrt{\frac{1}{20}}(n_1-n_4)-\sqrt{\frac{9}{20}}(n_2-n_3), \\
P^3_1 &= -\sqrt{\frac{1}{5}}B_{12}+\sqrt{\frac{3}{5}}B_{23}-\sqrt{\frac{1}{5}}B_{34}, \\
P^3_{-1} &= \sqrt{\frac{1}{5}}B_{21}-\sqrt{\frac{3}{5}}B_{32}+\sqrt{\frac{1}{5}}B_{43}, \\
P^3_2 &= \sqrt{\frac{1}{2}}(B_{24}-B_{13}) \quad P^3_{-2} = \sqrt{\frac{1}{2}}(B_{42}-B_{31}), \\
P^3_3 &= -B_{14} \quad P^3_{-3} = B_{41},
\end{aligned}
\tag{38}
$$

where the

$$
n_i = B_{ii} = \sum_{m_k} c^\dagger_{im_k} c_{im_k} - \frac{1}{4}\Omega \tag{39}
$$

are number operators for each of the four states and the total particle number n is the sum over the four states labeled by a in Table I, $n = n_1+n_2+n_3+n_4 =$ total particle number. It will be convenient notationally to sometimes replace the operator P^0_0 with the operator S_0, according to the relationship

$$
S_0 \equiv \tfrac{1}{2}(n-\Omega) = P^0_0, \tag{40}
$$

where 2Ω is the degeneracy of the space for the particles that participate in the SO(8) symmetry. Physically, $S_0 = \frac{1}{2}(n-\Omega)$ is one-half the particle number measured from half-filling (which corresponds to $n = \Omega$).

C. Lie algebra for coupled operators

Because the six operators defined by Eq. (34), their six hermitian conjugates, and the 16 operators defined by Eq. (36) are independent linear combinations of the SO(8) generators defined in Eqs. (14) and (15), the 28 operators $\{S, S^\dagger, D_\mu, D^\dagger_\mu, P^\ell_\mu\}$ also close an SO(8) algebra under commutation. The SO(8) commutation relations for the coupled representation $\{S, S^\dagger, D_\mu, D^\dagger_\mu, P^\ell_\mu\}$ are given explicitly by [18,31]

$$
[S, S^\dagger] = -2S_0, \tag{41a}
$$

$$
[D_{\mu'}, D^\dagger_\mu] = -2\delta_{\mu\mu'}S_0 + \sum_{t\ \text{odd}} (-1)^{\mu'} \times C^{t,\mu-\mu'}_{2,-\mu'2\mu} \begin{Bmatrix} 2 & 2 & t \\ \frac{3}{2} & \frac{3}{2} & \frac{3}{2} \end{Bmatrix} P^t_{\mu,-\mu'}, \tag{41b}
$$

$$
\left[D^\dagger_\mu, S\right] = P^2_\mu, \tag{41c}
$$

$$
\left[P^r_\mu, S^\dagger\right] = 2\delta_{r2}D^\dagger_\mu + 2\delta_{r0}\delta_{\mu 0}S^\dagger, \tag{41d}
$$

$$
[P^r_{\mu'}, D^\dagger_\mu] = 2(-1)^{\mu'}\delta_{r2}\delta_{-\mu\mu'} - 4\sqrt{5(2r+1)} \times C^{2,\mu+\mu'}_{r\mu'2\mu} \begin{Bmatrix} 2 & 2 & r \\ \frac{3}{2} & \frac{3}{2} & \frac{3}{2} \end{Bmatrix} D^\dagger_{\mu+\mu'}, \tag{41e}
$$

$$
\left[P^r_{\mu'}, P^s_\mu\right] = 2(-1)^{r+s}\sqrt{(2r+1)(2s+1)} \sum_t C^{t,\mu+\mu'}_{r\mu' s\mu} \times [1-(-1)^{r+s+t}] \begin{Bmatrix} r & s & t \\ \frac{3}{2} & \frac{3}{2} & \frac{3}{2} \end{Bmatrix} P^t_{\mu+\mu'}, \tag{41f}
$$

where S_0 is defined in Eq. (40) and $\{\}$ denotes the Wigner 6-j symbol [30] for the recoupling of three angular momenta to good total angular momentum.

XI. COLLECTIVE SUBSPACE

The action of the SO(8) pair creation operators on the pair vacuum N times creates a $2N$-particle state [31],

$$
|N_s N_d\rangle = (S^\dagger)^{N_s}(D^\dagger)^{N_d}|0\rangle, \tag{42}
$$

where the total number of pairs is $N = N_S + N_D$. The portion of the full Hilbert space that is spanned by the states (42) will be termed the *collective subspace*. It will play an important role in subsequent discussion where it will be shown that the SO(8) symmetry may be used to construct effective Hamiltonians that are diagonal in this space, and that the generators of SO(8) do not couple the subspace to the remainder of the space.

XII. ANALOGY WITH SO(8) SYMMETRY IN NUCLEI

The reason for our alternative labeling of the states in Table I in terms of the index m_i, and our particular choices of phases and normalizations in equations, can now be made clear. With these labelings and choices the six coupled particle-particle operators $S^\dagger$ and $D^\dagger_\mu$ defined in Eq. (34), their six hermitian conjugates S and D_μ, and the 16 coupled particle-hole operators P^ℓ_μ defined in Eq. (36), are mathematically in one-to-one correspondence with the 28 generators for the Ginocchio SO(8) model [31] and the SO(8) fermion dynamical symmetry model [16,17,32]. These have found

broad application in nuclear structure physics [18] and may be viewed as a microscopic justification for the interacting boson model (IBM) [33], which is one of the most commonly used phenomenological models in nuclear structure physics.

This correspondence has three important implications: (1) Mathematically, the group-theoretical methodology obtained for SO(8) already in nuclear physics applications may be appropriated for use in the graphene problem. (2) Physically, the nature of the generators for the nuclear physics and graphene SO(8) symmetries are fundamentally different, but analogs of physical interpretations applied already for nuclear physics SO(8) symmetries may shed light on the graphene problem. (3) Philosophically, the SO(8) correspondence between graphene and nuclear structure physics implies a satisfying convergence of mathematical reasoning and physical abstraction in two completely different scientific subfields. The third point will be elaborated in other papers; in this paper we concentrate on elucidating the first two points.

XIII. NUCLEAR ANALOG SUBGROUP CHAINS

The SO(8) group has various subgroups (subsets of generators closed under commutation) and these in turn may have other subgroups. These sequences of subgroups define subgroup chains. These chains will be discussed first in terms of the nuclear physics basis $\{S, S^\dagger, D_\mu, D^\dagger_\mu, P^\ell_\mu\}$, and then in terms of a new basis that is mathematically equivalent but is physically better suited to describing the physics of graphene.

In the nuclear physics, basis P^0 is the particle number and generates a group $\mathrm{U(1)_c}$, while P^1 is proportional to the total angular momentum and generates a group $\mathrm{SO(3)}_L$. In the nuclear physics context the total angular momentum and the particle number are expected to be conserved exactly for all physical states. Thus one seeks subgroup chains of SO(8) that end in the subgroup $\mathrm{SO(3)}_L \times \mathrm{U(1)_c}$ corresponding to charge and angular momentum conservation. Three SO(8) subgroup chains satisfy these conditions.

A. SO(5) × SU(2)$_\mathrm{p}$ subgroup chain

From Eq. (41a), the quasispin generators $(S, S^\dagger, S_0)$ close an $\mathrm{SU(2)_p}$ algebra that is a subalgebra of SO(8), and from Eq. (41d), the operators P^r_μ with $r = 1,3$ close an SO(5) algebra and commute with these SU(2) quasispin generators. Thus one subgroup of SO(8) is

$$\mathrm{SO(8)} \supset \mathrm{SO(5)} \times \mathrm{SU(2)_p},$$

where SO(5) is generated by the ten operators (P^1_μ, P^3_μ), where μ takes the $2r+1$ values $\mu = (-r, -r+1, \ldots, r-1, r)$ and the *quasispin group* $\mathrm{SU(2)_p}$ is generated by $(S, S^\dagger, S_0)$, where $S_0 = P^0$. Furthermore, the three generators P^1_μ are components of the total angular momentum L and generate an $\mathrm{SO(3)}_L$ subgroup of SO(5), and S_0 generates a $\mathrm{U(1)_c}$ subgroup of $\mathrm{SU(2)_p}$ corresponding to conservation of charge. Thus one subgroup chain is

$$\begin{aligned}\mathrm{SO(8)} \supset & \underset{\{P^1,\,P^3\}}{\mathrm{SO(5)}} \times \underset{\{S,\,S^\dagger,\,S_0\}}{\mathrm{SU(2)_p}} \supset \underset{\{P^1\}}{\mathrm{SO(3)}_L} \times \underset{\{S,\,S^\dagger,\,S_0\}}{\mathrm{SU(2)_p}} \\ & \supset \underset{\{P^1\}}{\mathrm{SO(3)}_L} \times \underset{\{S_0\}}{\mathrm{U(1)_c}}, \end{aligned} \tag{43}$$

where the generators of each subgroup are indicated in brackets below the subgroup and the product group on the last line corresponds to conservation of total angular momentum and particle number.

B. SO(6) ∼ SU(4) subgroup chain

The groups SU(4) and SO(6) share the same Lie algebra. In nuclear physics it is more common to refer to this group as SO(6), but to maintain a parallel with the ensuing treatment of graphene it will be labeled SU(4) in the present discussion. From Eq. (41f), the 16 operators $P^r_\mu (r = 0,1,2,3)$ are closed under commutation, corresponding to

$$\mathrm{SO(8)} \supset \mathrm{U(4)} \supset \mathrm{U(1)_c} \times \mathrm{SU(4)},$$

where the generator of $\mathrm{U(1)_c}$ is $P^0 = S_0$ and the 15 operators $P^r_\mu (r = 1,2,3)$ are the generators of SU(4). Furthermore, the subset of P^r with odd r are generators of the SO(5) symmetry discussed above and so generate an SO(5) subgroup of this SU(4) group. Hence a second subgroup chain is

$$\begin{aligned}\mathrm{SO(8)} \supset & \underset{\{P^0,\,P^1,\,p^2,\,P^3\}}{\mathrm{U(4)}} \supset \underset{\{S_0\}}{\mathrm{U(1)_c}} \times \underset{\{P^1,\,p^2,\,P^3\}}{\mathrm{SU(4)}} \\ & \supset \underset{\{P^1,\,P^3\}}{\mathrm{SO(5)}} \times \underset{\{S_0\}}{\mathrm{U(1)_c}} \supset \underset{\{P^1\}}{\mathrm{SO(3)}_L} \times \underset{\{S_0\}}{\mathrm{U(1)_c}}, \end{aligned} \tag{44}$$

where Eq. (40) has been used to replace P^0_0 with S_0.

C. SO(7) subgroup chain

From Eqs. (41b), (41e), and (41f), the 21 operators $\{S_0, D^\dagger_\mu, D_\mu, P^1_\mu, P^3_\mu\}$ close an SO(8) ⊃ SO(7) subalgebra of SO(8) and the subset $\{P^1, P^3, S_0\}$ closes an $\mathrm{SO(5)} \times \mathrm{U(1)_c}$ subalgebra of SO(7). Thus a third subgroup chain is given by

$$\begin{aligned}\mathrm{SO(8)} \supset & \underset{\{S_0,\,D^\dagger,\,D,\,P^1,\,P^3\}}{\mathrm{SO(7)}} \supset \underset{\{P^1,\,P^3\}}{\mathrm{SO(5)}} \times \underset{\{S_0\}}{\mathrm{U(1)_c}} \\ & \supset \underset{\{P^1\}}{\mathrm{SO(3)}_L} \times \underset{\{S_0\}}{\mathrm{U(1)_c}}. \end{aligned} \tag{45}$$

The relationships of the nuclear analog SO(8) subgroup chains described above are summarized in Fig. 7.

XIV. GRAPHENE SO(8) SUBGROUP CHAINS

The subgroup chains in Sec. XIII were expressed in terms of the nuclear physics basis $\{S, S^\dagger, D_\mu, D^\dagger_\mu, P^\ell_\mu\}$. This basis demonstrates the deep connection between graphene quantum Hall physics and nuclear structure physics, and is suitable mathematically to describe graphene quantum Hall effects. However, it is not well suited physically to interpreting the graphene quantum Hall effects for three reasons.

(1) The relationship between the generators of the SO(8) ⊃ SU(4) subgroup in the nuclear physics basis and those of the SU(4) quantum Hall ferromagnetism basis defined in Eq. (9) is not clear, which hinders interpretation of the present results in terms of preceding results found in the graphene literature.

(2) Charge and electronic spin are expected to be conserved in graphene (if the Zeeman term is neglected), but none

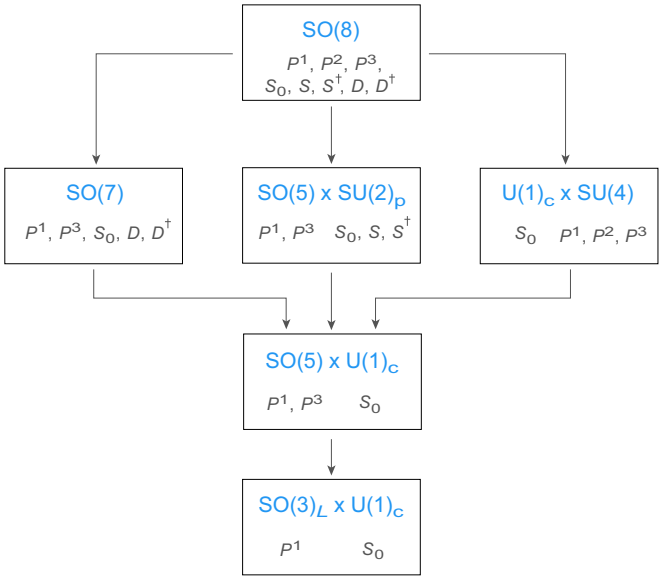

FIG. 7. Nuclear analog SO(8) subgroup chains with generators in the coupled representation $\{P^0, P^1, P^2, P^3, S, S^\dagger, D_\mu, D_\mu^\dagger\}$ given by Eqs. (36) and (34) and obeying the Lie algebra of Eq. (41). Generators are indicated below each group factor and S_0 and $P^0 \equiv P_0^0$ may be interchanged using Eq. (40). The subgroup structure expressed in this basis is in one-to-one correspondence with the SO(8) fermion dynamical symmetry model [17] of nuclear structure physics.

of the generators $\{S, S^\dagger, D_\mu, D_\mu^\dagger, P_\mu^\ell\}$ can be interpreted as spin in the application to graphene (instead, spin is a linear combination of these generators). For physical applications, it is desirable to employ a basis in which the relevant conservation laws are manifest.

(3) In addition to the exact conservation laws expected for charge and spin in graphene, it is expected on physical grounds that for low-energy excitations the scattering between valleys is strongly suppressed and the difference in electron densities between neighboring valleys should be very nearly conserved. This difference is expressed by the z component of the valley isospin T_z, and the corresponding approximate invariance is reflected in a $\mathrm{U(1)_v}$ symmetry generated by T_z. But T_z is not proportional to any of the P^r generators (it is a linear combination of these generators), so this approximate invariance is not manifest in the nuclear SU(4) basis.

Thus a new basis will be employed for the SO(8) generators in application to graphene for which the particle number (charge) operator n or S_0 and the 12 pairing operators $\{D_\mu, D_\mu^\dagger, S, S^\dagger\}$ are retained, but the 15 SU(4) generators $\{P^1, P^2, P^3\}$ in the nuclear representation are replaced with the 15 SU(4) generators $\{\mathcal{S}_\alpha, T_\alpha, N_\alpha, \Pi_{\alpha x}, \Pi_{\alpha y}\}$ with $\alpha = x, y, z$ defined in the graphene representation given in Eq. (9),

$$\{P^1, P^2, P^3, S_0, S, S^\dagger, D_\mu, D_\mu^\dagger\}_{\text{Nuclear SO(8)}} \longrightarrow$$
$$\{\mathcal{S}_\alpha, T_\alpha, N_\alpha, \Pi_{\alpha x}, \Pi_{\alpha y}, S_0, S, S^\dagger, D_\mu, D_\mu^\dagger\}_{\text{Graphene SO(8)}}.$$

The transformation from the $\{P^1, P^2, P^3\}$ generators to the $\{\mathcal{S}_\alpha, T_\alpha, N_\alpha, \Pi_{\alpha x}, \Pi_{\alpha y}\}$ generators is given in Appendix.

A. Order parameters

In the new basis, it will be convenient to take as order parameters

$$\langle \mathcal{S}_z \rangle = \langle \hat{n}_1 \rangle - \langle \hat{n}_2 \rangle + \langle \hat{n}_3 \rangle - \langle \hat{n}_4 \rangle, \tag{46a}$$
$$\langle T_z \rangle = \langle \hat{n}_1 \rangle + \langle \hat{n}_2 \rangle - \langle \hat{n}_3 \rangle - \langle \hat{n}_4 \rangle, \tag{46b}$$
$$\langle N_z \rangle = \langle \hat{n}_1 \rangle - \langle \hat{n}_2 \rangle + \langle \hat{n}_4 \rangle - \langle \hat{n}_3 \rangle, \tag{46c}$$

where $\hat{n}_i$ is the number operator counting particles in basis state $|i\rangle$ and the expectation value is taken with respect to the collective wave function. Physically, (1) the net spin is measured by $\langle \mathcal{S}_z \rangle$, which characterizes *ferromagnetic* order. (2) The difference in charge between the A and B sublattices is measured by $\langle T_z \rangle$, which characterizes *charge density wave* order. (3) The difference in spins between the A and B sublattices is measured by $\langle N_z \rangle$, which characterizes *antiferromagnetic* (Néel or spin density wave) order. The order parameters evaluated for the states of Fig. 6 are displayed in Table III.

B. Conserved quantities

In the new basis, it will be assumed that both charge and spin are exactly conserved for the physical states of the model in the absence of the Zeeman term H_Z, that the charge and the z component of spin are exactly conserved if the Zeeman term is included in the Hamiltonian, and that T_z is conserved, where appropriate. Neglecting the Zeeman term, the spin-charge symmetry corresponds to a group structure $\mathrm{SU(2)_\sigma \times U(1)_c}$, where $\mathrm{SU(2)_\sigma}$ is generated by the spin operators and $\mathrm{U(1)_c}$ is generated by the particle number operator. Thus one seeks subgroup chains of SO(8) that end in the subgroup $\mathrm{SU(2)_\sigma \times U(1)_c}$ corresponding to charge and spin conservation, and in some of these chains a $\mathrm{U(1)_v}$ subgroup implying conservation of T_z will also be required. The group and subgroup structure in the new basis is illustrated in Fig. 8, where seven nontrivial subgroup chains may be identified that begin with SO(8) and end with the symmetry $\mathrm{U(1)_c \times U(1)_s}$ corresponding to conservation of charge and z-component of the spin in the magnetic field

$$\mathrm{SO(8) \supset SU(4) \supset SO(5) \supset SU(2)}, \tag{47a}$$
$$\mathrm{SO(8) \supset SU(4) \supset SU(2)_\sigma^K \times SU(2)_\sigma^{K'} \supset SU(2)}, \tag{47b}$$
$$\mathrm{SO(8) \supset SU(4) \supset SU(2)_\sigma \times SU(2)_v \supset SU(2)}, \tag{47c}$$
$$\mathrm{SO(8) \supset SU(4) \supset SU(2)}, \tag{47d}$$
$$\mathrm{SO(8) \supset SO(5) \times SU(2)_p \supset SO(5) \supset SU(2)}, \tag{47e}$$
$$\mathrm{SO(8) \supset SO(5) \times SU(2)_p \supset SU(2)_\sigma \times SU(2)_p \supset SU(2)}, \tag{47f}$$
$$\mathrm{SO(8) \supset SO(7) \supset SO(5) \supset SU(2)}, \tag{47g}$$

where for brevity all U(1) factors are dropped in the notation and SU(2) means $\mathrm{SU(2)_\sigma}$ corresponding to conservation of spin. Each of these corresponds to a different dynamical

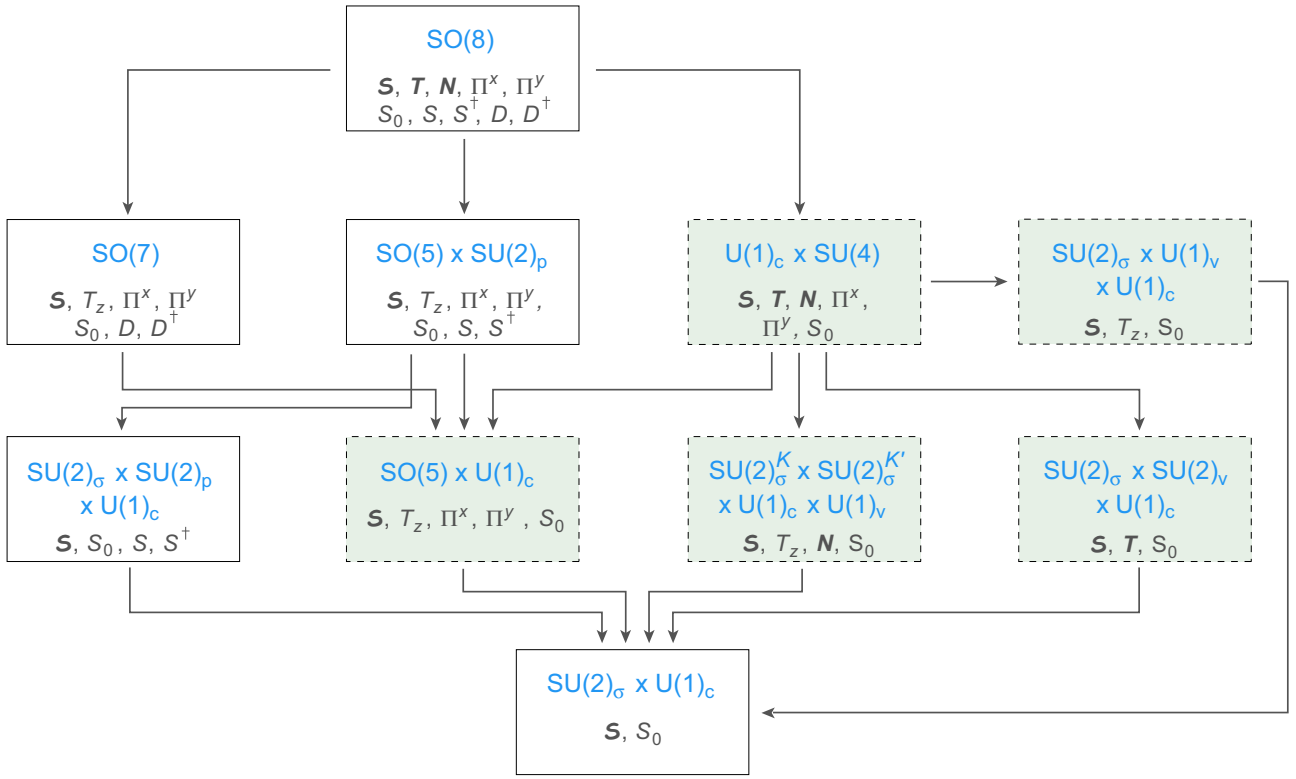

FIG. 8. SO(8) subgroup chains with generators in a representation more suitable than that of Fig. 7 for interpreting graphene physics. Group generators are indicated in each box. The boxes shown with shading and dashed boundaries and are relevant for interpreting the SU(4) quantum Hall ferromagnetism illustrated in Fig. 3. In this classification, the Zeeman term has been neglected so all subgroup chains end in the group $SU(2)_\sigma \times U(1)_c$ corresponding to the conservation of total spin and total charge. If the Zeeman term is included, it will influence directly only the spin sector and break all $SU(2)_\sigma$ factors down to $U(1)_\sigma$ generated by the z component of the spin, $\mathcal{S}_z$.

symmetry that is realized for particular choices of parameters for the SO(8) Hamiltonian, and that yields *exact many-body solutions* using the dynamical symmetry methodology. Let us now discuss in more detail three subgroup chains of SO(8).

C. The graphene SO(5) × SU(2) subgroup chains

The quasispin generators $(S, S^\dagger, S_0)$ close an $SU(2)_p$ algebra that is a subalgebra of SO(8), and the operators $\{\mathcal{S}_\alpha, \Pi_{\alpha x}, \Pi_{\alpha y}, T_z\}$ close an SO(5) algebra and commute with these SU(2) quasispin generators. Putting this together, one subgroup of SO(8) is $SO(8) \supset SO(5) \times SU(2)_p$, Furthermore, the three generators $\mathcal{S}_\alpha$ are components of the total spin and generate an $SU(2)_\sigma$ subgroup of SO(5), and S_0 generates a $U(1)_c$ subgroup of $SU(2)_p$ corresponding to conservation of charge. Thus one subgroup chain is

$$SO(8) \supset SO(5) \times SU(2)_p \supset SU(2)_\sigma \times SU(2)_p \supset SU(2)_\sigma \times U(1)_c, \quad (48)$$

where the product group on the last line corresponds to conservation of spin and charge. This subgroup chain with its corresponding generators is illustrated in Fig. 8. Alternatively, SO(5) may be broken according to the pattern

$$SO(8) \supset SO(5) \times SU(2)_p \supset SO(5) \times U(1)_c \supset SU(2)_\sigma \times U(1)_c, \quad (49)$$

which also conserves spin and charge, and is illustrated in Fig. 8.

D. The graphene SU(4) subgroup chains

A $U(4) \supset U(1)_c \times SU(4)$ subgroup of SO(8) may be obtained by removing the 12 pairing operators from the SO(8) generator set. The $U(1)_c$ subgroup is generated by the particle number (charge) and the SU(4) subgroup is generated by the 15 remaining operators, which are defined in Eq. (9) in the current basis. There are several options for chains corresponding to further subgroups.

(1) The subset $\{S_\alpha, \Pi_{\alpha x}, \Pi_{\alpha y}, T_z\}$ defines generators of the SO(5) symmetry discussed above and so forms an SO(5) subgroup of this SU(4) group. Hence one SU(4) subgroup chain is

$$SO(8) \supset U(4) \supset U(1)_c \times SU(4) \supset SO(5) \times U(1)_c \supset SU(2)_\sigma \times U(1)_c, \quad (50)$$

which is displayed in Fig. 8.

(2) Physically, the total spin is conserved. If there is little intervalley scattering one may also assume the spin within each K valley and each K' valley to be separately conserved, corresponding to a $SU(2)_\sigma^K \times SU(2)_\sigma^{K'}$ symmetry. Thus a second SU(4) subgroup chain

TABLE IV. Properties of SO(8) and its subgroups.[a]

Group[a]	Dim	Generators	Quantum numbers[b]	Casimir operators C_g	Casimir eigenvalues[c]
SO(8)	28	$P^1,P^2,P^3,S_0,S,S^\dagger,D,D^\dagger$	$\rho_1,\rho_2,\rho_3,\rho_4$	$\frac{1}{2}(S^\dagger S + D^\dagger\cdot D) + C_{SU(4)} + S_0(S_0-6)$	$\frac{1}{4}(\Omega-u)(\Omega-u+12)+\phi(\rho_i)$
SO(7)	21	$\{P^1,P^3,S_0,D,D^\dagger\}$ or $\{\boldsymbol{\Pi}_x,\boldsymbol{\Pi}_y,\boldsymbol{\mathcal{S}},\tau_z,S_0,D,D^\dagger\}$	$\theta_1,\theta_2,\theta_3$	$\frac{1}{2}\boldsymbol{D}^\dagger\cdot\boldsymbol{D} + S_0(S_0-5) + C_{SO(5)}$	$\frac{1}{2}(\Omega-w)(\Omega-w+10)+\zeta(\theta_i)$
SO(5)	10	$\{P^1,P^3\}$ or $\{\boldsymbol{\Pi}_x,\boldsymbol{\Pi}_y,\boldsymbol{\mathcal{S}},\tau_z\}$	τ,ω	$\boldsymbol{P}^1\cdot\boldsymbol{P}^1+\boldsymbol{P}^3\cdot\boldsymbol{P}^3 =$ $\boldsymbol{\Pi}_x\cdot\boldsymbol{\Pi}_x+\boldsymbol{\Pi}_y\cdot\boldsymbol{\Pi}_y+\frac{1}{4}\boldsymbol{\mathcal{S}}\cdot\boldsymbol{\mathcal{S}}+\frac{1}{4}\tau_z$	$\tau(\tau+3)+\frac{1}{2}\omega(\omega+4)+\tau\omega$
U(4)	16	P^0,P^1,P^2,P^3	$n,\sigma_1,\sigma_2,\sigma_3$	$\boldsymbol{P}^0\cdot\boldsymbol{P}^0+\boldsymbol{P}^1\cdot\boldsymbol{P}^1+\boldsymbol{P}^2\cdot\boldsymbol{P}^2+\boldsymbol{P}^3\cdot\boldsymbol{P}^3$	$n^2+\sigma(\sigma+4)$
SU(4)	15	$\{P^1,P^2,P^3\}$ or $\{\boldsymbol{\Pi}_x,\boldsymbol{\Pi}_y,\boldsymbol{N},\boldsymbol{\mathcal{S}},\boldsymbol{\tau}\}$	$\sigma_1,\sigma_2,\sigma_3$	$\boldsymbol{P}^1\cdot\boldsymbol{P}^1+\boldsymbol{P}^2\cdot\boldsymbol{P}^2+\boldsymbol{P}^3\cdot\boldsymbol{P}^3 =$ $\boldsymbol{\Pi}_x\cdot\boldsymbol{\Pi}_x+\boldsymbol{\Pi}_y\cdot\boldsymbol{\Pi}_y+\boldsymbol{N}\cdot\boldsymbol{N}+\frac{1}{4}(\boldsymbol{\mathcal{S}}\cdot\boldsymbol{\mathcal{S}}+\boldsymbol{\tau}\cdot\boldsymbol{\tau})$	$\sigma(\sigma+4)$
$SU(2)_p$	3	$S_0,S,S^\dagger$	ν	$S^\dagger S+S_0(S_0-1)$	$\frac{1}{4}(\Omega-\nu)(\Omega-\nu+2)$
$SU(2)_\sigma$	3	$\boldsymbol{\mathcal{S}}$	s	$\frac{1}{4}\boldsymbol{\mathcal{S}}\cdot\boldsymbol{\mathcal{S}}$	$s(s+1)$
$SU(2)_\tau$	3	$\boldsymbol{T}$	τ	$\frac{1}{4}\boldsymbol{T}\cdot\boldsymbol{T}$	$T(T+1)$
$U(1)_c$	1	S_0	n	S_0	$\frac{1}{2}(n-\Omega)$

[a]SU(4) ∼ SO(6) (they share the same Lie algebra). $S_0 = P^0 = \frac{1}{2}(n-\Omega)$, where n is particle number. Components of spin $\boldsymbol{\mathcal{S}}$ are functions of P^1 and P^3. The shorthand notation $\boldsymbol{\Pi}_\beta \equiv \Pi_{\alpha\beta}$ has been employed.

[b]The quantum numbers $\{\rho_i\}$, $\{\sigma_i\}$, $\{\theta_i\}$, and (τ,ω) are Dynkin labels [29] for the irreps of SO(8), SU(4), SO(7), and SO(5), respectively; see Ref. [28]. The SO(7) quantum number w appearing in the Casimir eigenvalue is the number of particles that do not form D pairs (see the $D^\dagger_\mu$ creation operators defined in Eq. (34). The seniority quantum number ν is the number of particles that do not form S pairs.

[c]The number of particles not coupled to S or D pairs is u. The functions $\phi(\rho_i)$ and $\zeta(\theta_i)$ are given by [18]

$$\phi(\rho_1,\rho_2,\rho_3) = \tfrac{1}{2}\left(\rho_1^2+\rho_2^2\right)+\tfrac{1}{4}(\rho_1+\rho_3)(\rho_1+\rho_3+4\rho_2+12)+\rho_2(\rho_2+4)$$
$$\zeta(\theta_2,\theta_3) = \theta_2(\theta_2+3)+\tfrac{1}{2}\theta_3(\theta_3+4)+\theta_2\theta_3$$

They are nonzero only if $u \neq 0$.

corresponds to

$$\begin{aligned}\mathrm{SO(8)} &\supset \mathrm{U(4)} \supset \mathrm{U(1)_c}\times\mathrm{SU(4)}\\ &\supset \mathrm{SU(2)}_\sigma^K \times \mathrm{SU(2)}_\sigma^{K'} \times \mathrm{U(1)_c}\times\mathrm{U(1)_v}\\ &\supset \mathrm{SU(2)}_\sigma \times \mathrm{U(1)_c},\end{aligned} \tag{51}$$

where $U(1)_v$ is generated by T_z. This chain also is displayed in Fig. 8.

(3) Finally, one can imagine that SU(4) is broken into subgroups corresponding to simultaneous conservation of both spin and valley isospin, giving a third SU(4) subgroup chain,

$$\begin{aligned}\mathrm{SO(8)} &\supset \mathrm{U(4)} \supset \mathrm{U(1)_c}\times\mathrm{SU(4)}\\ &\supset \mathrm{SU(2)}_\sigma \times \mathrm{SU(2)_v}\times\mathrm{U(1)_c} \supset \mathrm{SU(2)}_\sigma\times\mathrm{U(1)_c},\end{aligned} \tag{52}$$

as illustrated in Fig. 8.

Comparing Fig. 8 with Fig. 3, it is apparent that the three SO(8) ⊃ SU(4) subgroup chains defined in this section correspond to the three symmetry-breaking patterns described in Sec. VI and discussed in Refs. [26,27] for the SU(4) quantum Hall ferromagnetism model. The portion of the SO(8) subgroup structure leading to SU(4) quantum Hall ferromagnetism is indicated by the shaded boxes with dashed outer boundaries in Fig. 8. Thus it is seen explicitly that the special case corresponding to the SO(8) ⊃ SU(4) subgroup chains of the present model imply the results of Refs. [26,27].

E. The graphene SO(7) subgroup chain

The 21 operators $\{\mathcal{S}_\alpha, \Pi_{\alpha x}, \Pi_{\alpha y}, T_z, S_0, D^\dagger_\mu, D_\mu\}$ close an SO(8) ⊃ SO(7) subalgebra of SO(8), and the subset of generators $\{\mathcal{S}_\alpha, \Pi_{\alpha x}, \Pi_{\alpha y}, T_z, S_0\}$ close an SO(5) × U(1)$_c$ subalgebra of SO(7). Thus a third subgroup chain is given by

$$\begin{aligned}\mathrm{SO(8)} &\supset \mathrm{U(4)} \supset \mathrm{U(1)_c}\times\mathrm{SU(4)}\\ &\supset \mathrm{SO(7)} \supset \mathrm{SO(5)}\times\mathrm{U(1)_c} \supset \mathrm{SU(2)}_\sigma\times\mathrm{U(1)_c},\end{aligned} \tag{53}$$

as illustrated in Fig. 8. This subgroup chain is of particular interest because it will define a *critical dynamical symmetry* that represents an entire phase exhibiting critical behavior and interpolating between two other phases.

XV. DYNAMICAL SYMMETRY LIMITS

Let us use the subgroup structure of the preceding section to obtain exact solutions of the correlated many-body problem in these dynamical symmetry limits. The basic idea is to use the Casimir invariants of the subgroup chains like those described in Sec. XIV and illustrated in Fig. 8 to label states. Then model Hamiltonians constructed only from the Casimir invariants of a single subgroup chain permit analytical solution of the effective Schrödinger equation in that symmetry limit [18]. Specifically, if a Hamiltonian $H = f(C_1,C_2,\ldots,C_n)$ can be expressed as a function of the Casimir invariants of some subgroup chain $G_1 \supset G_2 \supset \cdots \supset G_n$, where the C_i represent Casimir operators for the groups G_i, then the system is said to possess a dynamical symmetry associated with the subgroup chain.

The discussion will be simplified by restricting to the lowest-order Casimir invariant for each group, which corresponds physically to omitting n-body interactions with $n > 2$. Elementary properties of Lie groups then permit the

eigenvalues E and eigenfunctions Ψ of this Hamiltonian to be expressed in closed form as

$$E = f(C_1(\nu_1), C_2(\nu_2), \ldots, C_n(\nu_n)) \quad \Psi = |\nu_1, \nu_2, \ldots, \nu_n\rangle,$$

where the ν_i stand for the quantum numbers required to specify the irreducible representations (irreps) of the groups G_i. The physical properties of the corresponding states can then be elucidated by using the methods of Lie groups and Lie algebras to evaluate matrix elements for observables. In this way, one generally finds that the dynamical symmetries associated with subgroup chains of some highest symmetry define collective (emergent) states that correspond to particular patterns of spontaneous symmetry breaking.

The Casimir operators that appear in each of these subgroups chains and the relevant quantum numbers labeling the states for each dynamical symmetry are summarized in Table IV. In the next section, these results for the Casimir operators will be used to construct the most general Hamiltonian permitted in the truncated collective space for specific dynamical symmetries.

A. Most general dynamical symmetry Hamiltonian

As has been seen, in a particular dynamical symmetry limit the most general Hamiltonian can be constructed from a sum of Casimir invariants for the groups contained in the corresponding subgroup chain. For SO(8) dynamical symmetries, the most general Hamiltonian in the absence of the Zeeman term is represented by the linear combination

$$H = H_0 + aC_{\mathrm{SO}(8)} + bC_{\mathrm{SU}(4)} + cC_{\mathrm{SO}(5)} + dC_{\mathrm{SU}(2)_\mathrm{p}} + eC_{\mathrm{SU}(2)_\sigma},$$

where H_0 is assumed constant in the symmetry limit, the Casimir operators C_g have been summarized in Table IV, and $C_{\mathrm{SO}(7)}$ does not appear explicitly because it has been eliminated by the constraint [17]:

$$C_{\mathrm{SO}(7)} = C_{\mathrm{SO}(8)} - C_{\mathrm{SU}(4)} + C_{\mathrm{SO}(5)} - S^\dagger S + S_0. \tag{54}$$

Hamiltonians representing specific dynamical symmetry limits then correspond to particular choices of the coefficients $a, b, \ldots$ in this general expression. It may be shown that the most general Hamiltonian can also be expressed in the compact form (see Eqs. (4.1) of Ref. [17])

$$H = H_0' + G_0 S^\dagger S + G_2 D^\dagger \cdot D + \sum_{r=1,2,3} B_r P^r \cdot P^r, \tag{55}$$

where H_0' is assumed constant in a symmetry limit and where the different dynamical symmetry limits correspond to specific choices for the values of the parameters G_0, G_2, and B_r. The last term is expressed in terms of the P^r from the nuclear basis. It can be converted to the graphene basis by inverting Eq. (A1) of Appendix to solve for the P^r.

Let us now discuss each of the SO(8) dynamical symmetries and their physical interpretations. For brevity, let us refer to the following. (1) The dynamical symmetry structure associated with Eqs. (48) and (49) as the SO(5) × SU(2) *dynamical symmetry*. (2) The dynamical symmetry structure associated with Eqs. (50)–(52) as the SU(4) *dynamical symmetry*. (3) The dynamical symmetry structure associated with Eq. (53) as the SO(7) *dynamical symmetry.*

Initially, the role of the Zeeman term (which would break the full spin symmetry down to conservation of its z component) will be ignored and it will be assumed that the chains end in the subgroup $\mathrm{SU}(2)_\sigma \times \mathrm{U}(1)_\mathrm{c}$ corresponding to the physical requirement that spin and charge be conserved exactly.

B. The SO(5) × SU(2) dynamical symmetry

The dynamical symmetry chains given in Eqs. (48)–(49) and illustrated in Fig. 8 correspond to two alternative ways of choosing subgroups of $\mathrm{SO}(5) \times \mathrm{SU}(2)_\mathrm{p}$:

$$\begin{array}{ccccc} & \curvearrowright & \mathrm{SU}(2)_\sigma \times \mathrm{SU}(2)_\mathrm{p} & \curvearrowright & \\ \mathrm{SO}(5) \times \mathrm{SU}(2)_\mathrm{p} & & & & \mathrm{SU}(2)_\sigma \times \mathrm{U}(1)_\mathrm{c} \\ & \curvearrowright & \mathrm{SO}(5) \times \mathrm{U}(1)_\mathrm{c} & \curvearrowright & \end{array}.$$

In the upper branch of the middle step, the SO(5) symmetry is broken to its SU(2) spin subgroup, with $\mathrm{SU}(2)_\mathrm{p}$ unbroken. Physically, this corresponds to conservation of the spin associated with the S_α angular momentum algebra and the pseudospin associated with the $\{S, S^\dagger, S_0\}$ pair algebra, but not the full SO(5) symmetry. In the lower branch of the middle step, the SO(5) symmetry remains intact and S-pair pseudospin SU(2) is broken to U(1) charge. In the final subgroup of both chains, only the spin and charge remain as conserved quantities.

The Hamiltonian in the SO(5) × SU(2) dynamical symmetry limit corresponds to Eq. (55) with the restriction that $G_2 = B_2 = 0$,

$$\begin{aligned} H_{\mathrm{SO}(5)} &= G_0 S^\dagger S + \sum_{r=1,3} B_r P^r \cdot P^r \\ &= \mathbf{\Pi}_x \cdot \mathbf{\Pi}_x + \mathbf{\Pi}_y \cdot \mathbf{\Pi}_y + \frac{1}{4}\boldsymbol{\mathfrak{S}} \cdot \boldsymbol{\mathfrak{S}} + \frac{1}{4}\tau_z^2 \\ &= \frac{1}{4}\sum \boldsymbol{\sigma}^i \cdot \boldsymbol{\sigma}^j \left(\tau_x^i \tau_x^j + \tau_y^i \tau_y^j\right) \\ &\quad + \frac{1}{4}\sum \boldsymbol{\sigma}^i \cdot \boldsymbol{\sigma}^j + \frac{1}{4}\sum \tau_z^i \tau_z^i, \end{aligned} \tag{56}$$

where terms that are constant within a given representation have been omitted and $\mathbf{\Pi}_\beta \equiv \Pi_{\alpha\beta}$.

The most general SO(8) state in the $u = 0$ collective subspace is given by Eq. (42) and corresponds to a superposition of S and D_μ pairs. Schematically,

$$|\mathrm{SO}(8)\rangle = (S^\dagger)^{N-N_d}(D^\dagger)^{N_d}|0\rangle, \tag{57}$$

with $S^\dagger$ and $D^\dagger$ defined in Eq. (34) and $N_d \leqslant N$, where N is the total pair number. On the other hand, the most general states corresponding to the various subgroup chains illustrated in Fig. 8 correspond to pair superpositions having specific constraints on the relative contribution of S and D pairs. The collective subspace for the $\mathrm{SO}(5) \times \mathrm{SU}(2)_\mathrm{p}$ subgroup of SO(8) is of the form (see Eq. (9.13) of Ref. [31])

$$|\mathrm{SO}(5) \times \mathrm{SU}(2)_\mathrm{p}\rangle = (S^\dagger)^N|0\rangle, \tag{58}$$

implying that it is a superposition of S pairs. Conceptually, the wave function of the $\mathrm{SO}(5) \times \mathrm{SU}(2)_\mathrm{p}$ subgroup chain for

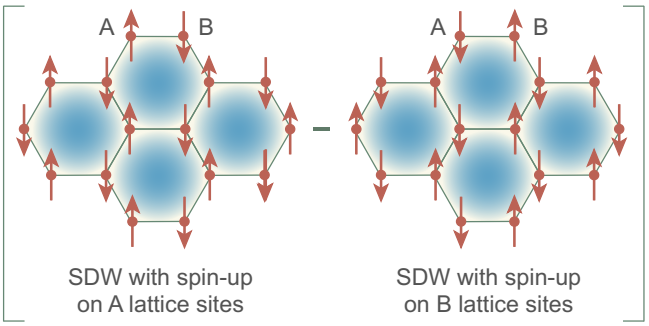

FIG. 9. The collective state corresponding to the SO(8) ⊃ SO(5) × SU(2) ground state. The state is an antisymmetric combination of a spin density wave with spin up on the A lattice sites and spin down on the B sites, and a spin density wave with spin up on the B sites and spin down on the A sites.

$u = 0$ is obtained from the most general state in the collective subspace by converting all of its D pairs to S pairs.

As was seen in Sec. X A and Fig. 6, the S and D pairs correspond to coherent superpositions of particular electronic distributions in spin and valley pseudospin. Thus specific S and D pair content for SO(8) dynamical symmetry subgroup chains implies specific collective modes associated with coherent distribution of the electrons in spin and valley space. It has been noted above that in the SO(5) × SU(2) dynamical symmetry limit the ground states correspond to a superposition of S pairs. The nature of this collective state may be inferred from Fig. 6 and is illustrated in Fig. 9.

C. The SU(4) dynamical symmetry

The SU(4) dynamical symmetry corresponds to the three SO(8) subgroup chains

$$\begin{aligned}
&\mathrm{U(1)_c} \times \mathrm{SU(4)} \supset \mathrm{SO(5)} \times \mathrm{U(1)_c} \supset \mathrm{SU(2)_\sigma} \times \mathrm{U(1)_c},\\
&\mathrm{U(1)_c} \times \mathrm{SU(4)} \supset \mathrm{SU(2)_\sigma^K} \times \mathrm{SU(2)_\sigma^{K'}} \times \mathrm{U(1)_c} \times \mathrm{U(1)_v}\\
&\qquad\qquad \supset \mathrm{SU(2)_\sigma} \times \mathrm{U(1)_c},\\
&\mathrm{U(1)_c} \times \mathrm{SU(4)} \supset \mathrm{SU(2)_\sigma} \times \mathrm{SU(2)_v} \times \mathrm{U(1)_c}\\
&\qquad\qquad \supset \mathrm{SU(2)_\sigma} \times \mathrm{U(1)_c},
\end{aligned}$$

that were introduced in Eqs. (50)–(52) and Fig. 8. As already noted, these three dynamical symmetry chains are in one to one correspondence with the explicit symmetry breaking patterns that have been identified for SU(4) quantum Hall ferromagnetism. The most general SU(4) wave function for N pairs in the $u = 0$ collective SO(8) subspace is given by [31]

$$|\mathrm{SU(4)}\rangle = \sum_{p=1}^{N/2} \beta_p (S^\dagger)^{N-2p} [(S^\dagger)^2 - D^\dagger \cdot D^\dagger]^p |0\rangle, \qquad (59)$$

which corresponds physically to a restriction of the general SO(8) wave function (57) to a specific superposition of S and D pairs. The wave function for the SO(5) × U(1)$_c$ subgroup of SU(4) is given by Eq. (58). The wave function of the parent SU(4) group is a superposition of S and D pairs but the SO(5) × SU(2) subgroup has a wave function containing only S pairs.

D. The SO(7) dynamical symmetry

The SO(7) dynamical symmetry corresponds to the SO(8) subgroup chain

$$\mathrm{SO(7)} \supset \mathrm{SO(5)} \times \mathrm{U(1)_c} \supset \mathrm{SU(2)_\sigma} \times \mathrm{U(1)_c}$$

that was introduced in Eq. (53) and displayed in Fig. 8. The Hamiltonian in the SO(7) dynamical symmetry limit corresponds to Eq. (55) with the restriction that $G_0 = B_1 = B_2 = B_3 = 0$,

$$H_{\mathrm{SO(7)}} = G_0 S^\dagger S + \sum_{r=1,3} B_r \, P^r \cdot P^r, \qquad (60)$$

where terms have been dropped that are constant within a given representation.

From the nuclear physics analog SO(8) symmetry [18], it may be surmised that SO(7) will play the role of a *critical dynamical symmetry* interpolating smoothly between the collective states corresponding to the SU(4) dynamical symmetry and the collective states corresponding to SO(5) dynamical symmetry. Such critical dynamical symmetries have been discussed previously in both nuclear physics [18,34,35] and for the strongly correlated electrons leading to cuprate and iron-based high-temperature superconductivity [19,20]. They may be viewed as the generalization of a quantum critical point to an entire *quantum critical phase,* and may represent a fundamental organizing principle for quantum critical behavior. The physical implications of this SO(7) critical dynamical symmetry for graphene quantum Hall physics will be discussed further below.

XVI. GENERALIZED COHERENT STATES

The dynamical symmetry limits discussed above represent special solutions resulting from particular choices of the coupling parameters appearing in the Hamiltonian. For arbitrary choices of the coupling parameters the solutions will correspond generally to superpositions of the different symmetry-limit solutions and will not have exact analytical forms. In this more general case, it is quite feasible to obtain solutions numerically, since the collective subspace is highly truncated relative to the full Hilbert space. However, there is a powerful alternative approach: the *generalized coherent state approximation,* which permits *analytical solutions* for arbitrary choices of the coupling parameters in the Hamiltonian.

For the SO(8) Lie algebra introduced in this paper for graphene, the Gilmore-Perelomov algorithm [36–40] may be implemented to obtain solutions in terms of a set of generalized coherent states. These solutions represent the most general Hartree-Fock-Bogoliubov theory that can be formulated in the space, subject to a dynamical symmetry constraint [32]. The solutions of this Symmetry-Constrained Hartree-Fock-Bogoliubov (SCHFB) theory correspond to determining the stable points of energy surfaces, which represent the coherent-state expectation values of the effective Hamiltonian on the coset space. Thus the coherent state solutions also represent a microscopically derived implementation of Ginzburg-Landau theory. These coherent state solutions are uniquely well suited to study the interplay of competing spontaneous symmetry breaking in determining the ground state of the system and

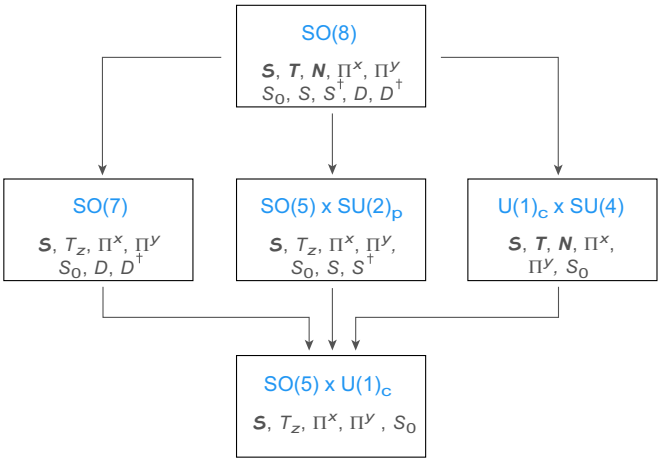

FIG. 10. Subgroup chains included in the present coherent state analysis.

its properties, and have been shown to give quantitative descriptions of data in a variety of fields [18,40].

A. Constructing SO(8) coherent states

The coherent states associated with the full set of subgroup chains in Fig. 8 will be discussed in future work. In this paper, the power of the method will be illustrated succinctly by restricting to the coherent states associated with the subgroup chains of SO(8) that contain the SO(5) subgroup, as illustrated in Fig. 10. Thus the corresponding coherent state solutions will represent a superposition of the symmetry-limit solutions for the

$$\mathrm{SO}(8) \supset \mathrm{SO}(5) \times \mathrm{SU}(2)_{\mathrm{p}} \supset \mathrm{SO}(5),$$
$$\mathrm{SO}(8) \supset \mathrm{SU}(4) \supset \mathrm{SO}(5), \qquad \mathrm{SO}(8) \supset \mathrm{SO}(7) \supset \mathrm{SO}(5)$$

dynamical symmetries. These coherent state solutions will be seen to have the following properties. (1) The SO(7) dynamical symmetry will play the role of a critical dynamical symmetry interpolating between SU(4) and SO(5) symmetry-limit solutions. (2) Because of fundamental symmetries obeyed by the wave function, the coherent state solutions may be parameterized in terms of a single collective parameter β that governs the mixture of the S and D pairs defined in Eq. (34) contributing in the ground state. (3) The collective parameter β may also be interpreted physically in terms of the pair configurations displayed in Fig. 6. The SO(8) coherent states corresponding to the symmetry structure in Fig. 10 have been developed previously in Ref. [35] for nuclear physics applications and will be adapted extensively to development of the present formalism.

B. SO(8) coherent state energy surfaces

Let us now consider the energy surfaces that may be computed from the coherent states, which link the SO(8) solutions to Ginzburg-Landau theory. Within the coherent state formalism the ground state energy may be determined through the variational requirement $\delta\langle\eta|H|\eta\rangle = 0$, where $|\eta\rangle$ is the coherent state, H is the SO(8) Hamiltonian,

$$H = H' + G_0 S^\dagger S + \sum_{r=1,2,3} b_r P^r \cdot P^r, \tag{61}$$

and the coefficients G_0 and b_r are functions of the effective interaction. For the dynamical symmetry chains having SO(5) as a subgroup the energies take the general form [35]

$$E_{\mathrm{g}}(n,\beta) = N_{\mathrm{g}}[A_{\mathrm{g}}\beta^4 + B_{\mathrm{g}}(n)\beta^2 + C_{\mathrm{g}}(n) + D_{\mathrm{g}}(n,\beta)], \tag{62}$$

where the group-dependent parameters N_{g}, A_{g}, $B_{\mathrm{g}}(n)$, $C_{\mathrm{g}}(n)$, and $D_{\mathrm{g}}(n,\beta)$ are given in Table V.

Our primary interest in this discussion is in the ground state properties of graphene in a strong magnetic field. The ground states in the coherent state approximation at fixed $n/2\Omega$ will be given by those values of $\beta \equiv \beta_0$ that correspond to minima of the energy surface $E(n,\beta)$. These are determined by the values of β satisfying

$$\frac{\partial E_{\mathrm{g}}(n,\beta))}{\partial\beta} = 0 \qquad \frac{\partial^2 E_{\mathrm{g}}(n,\beta))}{\partial\beta^2} > 0. \tag{63}$$

Evaluating these constraints for the energy surfaces (62), one finds that the minima β_0^{g} are given by [35]

$$\beta_0^{\mathrm{SU(2)\times SO(5)}} = \beta_0^{\mathrm{SO(7)}} = 0 \qquad \beta_0^{\mathrm{SU(4)}} = \pm\sqrt{\frac{n}{4\Omega}}. \tag{64}$$

The coherent state energy surfaces for the SO(5) × SU(2), SO(7), and SU(4) symmetry limits computed from Eq. (62) using the entries in Table V are shown as functions of β for several values of the fractional occupation f in Fig. 11. There one sees that indeed the minima for the SO(5) × SU(2) and SO(7) limits are at $\beta_0 = 0$, and the minima for the SU(4) limit are at $\beta_0 = \pm\sqrt{n/4\Omega}$.

Although the minimum energies for both the SO(5) × SU(2) and SO(7) limits are consistent with $\beta_0 = 0$, Fig. 11 shows that these symmetries differ fundamentally in the localization of the minimum. For SO(5) × SU(2), the energy surface has a deep minimum at $\beta_0 = 0$ but for SO(7) the energy surface is very flat around $\beta_0 = 0$, with a broad range of β giving essentially the same ground state energy. This highly degenerate SO(7) ground state has significant physical implications that will be discussed further below.

XVII. ELEMENTARY CONSERVATION LAWS

The SO(8) generalized coherent state is equivalent to the Hartree-Fock-Bogoliubov (HFB) approximation subject to a symmetry constraint. Since HFB is a BCS-type approximation married to a Hartree-Fock mean field, its solutions correspond to symmetry-breaking intrinsic states. In particular, the BCS-like state conserves the physical particle number only on average, and the Hartree-Fock mean field may break both translational and rotational invariance. Let us address these issues for the SO(8) coherent state.

The fractional uncertainty in electron number Δn for the SO(8) coherent state is given by [35]

$$(\Delta n)^2 = \langle\hat{n}^2\rangle - \langle\hat{n}\rangle = 2n - \frac{n^2}{\Omega} + 16\Omega\beta_0^4 - 8n\beta_0^2, \tag{65}$$

where β_0 is the value of β at the minimum energy, given by Eq. (64) in the symmetry limits. Expressing Eq. (65) in terms

TABLE V. Parameters for the energy surfaces $E_g(n,\beta)$ defined in Eq. (62).

g	N_g	A	$B(n)$	$C(n)$	$D(n,\beta)$[†a]
SU(2)	G_0	$2\Omega(\Omega-2)$	$-n(\Omega-2)$	$n\left(\Omega-\frac{1}{2}n+\frac{n}{\Omega}\right)/4$	$\frac{1}{2}\Omega^2F(n,\beta)$
SO(5)	b_3	-8Ω	$4n$	$n\left(1-\frac{n}{2\Omega}\right)$	$-2\Omega F(n,\beta)$
SU(4)	b_2	$-4\Omega(\Omega+3)$	$2n(\Omega+3)$	$\frac{5}{4\Omega}(2\Omega-n)$	0
SO(7)	G_2	$2\Omega(\Omega+4)$	$-n(\Omega+4)$	$-\frac{n}{4}\left(\Omega-\frac{n}{2}-\frac{2n}{\Omega}+4\right)+\frac{\Omega}{4}(\Omega+10)$	$-\frac{1}{2}\Omega(\Omega+4)F(n,\beta)$

[a]The function $F(n,\beta)$ is defined by $F(n,\beta)\equiv(\frac{n}{2\Omega}-2\beta^2)[(1-\frac{n}{2\Omega})^2-4(\frac{n}{2\Omega}-\beta^2)\beta^2]^{1/2}$.

of the fractional occupation $f=n/2\Omega$, in the SO(5) × SU(2) and SU(4) limits, respectively, one obtains

$$\left[\frac{\Delta n}{n}\right]_{\mathrm{SO_5\times SU(2)}}=\sqrt{\frac{1-f}{f\Omega}},\qquad \left[\frac{\Delta n}{n}\right]_{\mathrm{SU_4}}=\sqrt{\frac{1-2f}{f\Omega}}. \quad (66)$$

These results illustrate two important things. (1) The fluctuation in particle number is large at low degeneracy Ω but decreases with increasing Ω. (2) If SU(4) symmetry is realized $\Delta n/n$ decreases with increasing f and *vanishes identically* at $f=\frac{1}{2}$ for any Ω, which corresponds to the fractional occupation for the ground state of undoped graphene.

Thus it is expected that the current theory applied to graphene has negligible particle number fluctuation $\Delta n/n$ in the SU(4) limit. In the SO(5) × SU(2) limit, the particle number fluctuation $\Delta n/n$ remains finite for all f but it becomes very small as Ω becomes large, particularly near $f=\frac{1}{2}$. Thus it too may be neglected in the large-Ω limit. Comparison with Table II suggests that graphene quantum Hall experiments involve sufficient degeneracy that particle number fluctuation in the coherent state solution is not significant.

The coherent state approximation represents a mean field localized in spatial position and orientation, so it violates translational and rotational invariance. However, because the crystal is generally macroscopic, the net symmetry violation may be expected to be negligible. One concludes that for applications of coherent state methods to graphene, violations of particle number conservation, rotational invariance, and translational invariance are negligible in realistic systems.

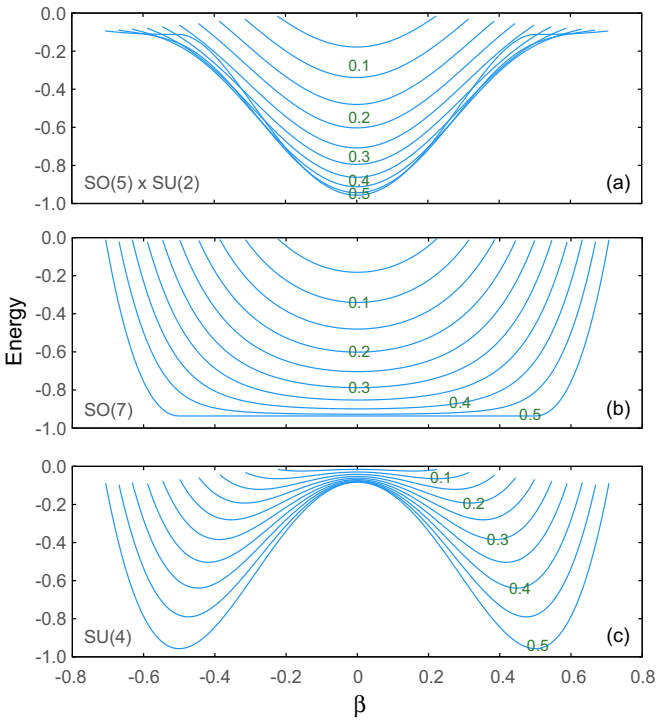

FIG. 11. Coherent state energy surfaces as a function of the order parameter β for three of the SO(8) dynamical symmetry limits. The curves are labeled by the fractional occupation $f=n/2\Omega$ defined in Eq. (23), where n is the particle number and 2Ω is the maximum number of particles that can be accommodated in the Landau level. The formalism is particle-hole symmetric so curves for fractional occupations with $f>\frac{1}{2}$ are equivalent to those shown above, but with the fractional occupation counted in terms of number of holes. For example, the curves for $f=0.4$ and 0.6 are equivalent. For the direct product group SU(2) × SO(5) the energy surface is the sum of contributions to Eq. (62) from SU(2) and SO(5). As will be demonstrated later, the SU(2) contribution typically dominates that of SO(5).

XVIII. COHERENT-STATE WAVE FUNCTIONS AND ORDER PARAMETERS

The generalized coherent state method has been used above to calculate total energy surfaces for quantum Hall states in graphene, but one also may use the coherent state wave functions and appropriate operators to calculate matrix elements of other relevant observables. This section addresses the nature of the wave function and the matrix elements that can serve as order parameters.

A. Order parameters

A significant consequence of the SO(8) dynamical symmetry structure displayed in Fig. 10 is that the phases may be distinguished in terms of a single order parameter and its fluctuations, which may be taken to be β. Let us now characterize in more depth the physical meaning of this order parameter. In Sec. XIV A, an antiferromagnetic order parameter $\langle N_z\rangle$ was defined. In the coherent state approximation the onset of AF order is signaled by an energy-surface minimum at a finite value of β. Because $N_z=P_0^2$ [see Eq. (A1i)], the antiferromagnetic order parameter $\langle N_z\rangle$ is related to the coherent state AF order parameter β by the intrinsic state matrix element of P_0^2 [35],

$$\begin{aligned}\langle N_z\rangle &= |b_2|\langle \mathrm{int},\beta,\gamma,n|P_0^2|\mathrm{int},\beta,\gamma,n\rangle\\ &= 2\Omega|b_2|(f-\beta^2)^{1/2}\,\beta, \end{aligned}\quad (67)$$

where b_2 is the coupling strength for the $P^2 \cdot P^2$ term in the Hamiltonian. Each value of β corresponds to a unique value of $\langle N_z \rangle$, so β is a measure of antiferromagnetic order.

The location of the maxima may be obtained by setting the derivative with respect to β of Eq. (67) equal to zero, which yields that $\langle N_z \rangle_{\max}$ for a given n occurs at a β of

$$\beta = \sqrt{\frac{n}{4\Omega}} = \beta_0^{\mathrm{SU}(4)}, \tag{68}$$

where Eq. (64) was used to make the identification in the last step. Thus, if $\beta \neq 0$, the maximum value of $\langle N_z \rangle$ maps to a value of β that corresponds to a minimum of the energy surface (a ground state) in the SU(4) limit. Substituting Eq. (64) for β in Eq. (67), for $\beta \neq 0$, ground states the AF order parameter $\langle N_z \rangle$ depends on the electron number n as

$$\langle N_z \rangle_{\max} = 2\Omega|b_2|\left(\frac{n}{4\Omega}\right) = \Omega|b_2|f. \tag{69}$$

The SO(8) model is particle-hole symmetric so n or f count electrons up to half-filling and holes for greater than half-filling. Hence the maximum AF collectivity occurs for half-filling of the single valence Landau level.

B. Coherent State wave functions

As was discussed in Sec. XVII, the coherent state wave function corresponding physically to $N = 2n$ pairs conserves particle number only on average and so is a superposition of terms having different numbers of pairs. In Eq. (5.27) of Ref. [35], the SO(8) coherent state is decomposed into terms of definite pair number p according to

$$|\beta\rangle = \sum_p C_p (S^\dagger + \kappa D_0^\dagger)^p |0\rangle, \tag{70}$$

where $|\beta\rangle$ denotes an intrinsic state with order parameter β and closed forms for C_p and κ are given in Ref. [35]. According to Eq. (5.28) of Ref. [35], the values of κ that correspond to the minima of the potential energy surface at $\beta = 0$ for the SO(5) × SU(2) limit and $\beta = \pm\sqrt{n/4\Omega}$ for the SU(4) limit [see Eq. (64)], respectively, are

$$\kappa_{\mathrm{SO}_5\times\mathrm{SU}_2} = 0, \qquad \kappa_{\mathrm{SU}(4)} = \pm 1, \tag{71}$$

so the SO(8) coherent state wave function (70) in the SO(5) × SU(2) and SU(4) limits, respectively, becomes

$$\begin{aligned} |\mathrm{SO}_5 \times \mathrm{SU}_2\rangle &= \sum_p C_p (S^\dagger)^p |0\rangle, \\ |\mathrm{SU}_4\rangle &= \sum_p C_p (S^\dagger \pm D_0^\dagger)^p |0\rangle = 2\sum_p C_p (Q_\pm^\dagger)^p |0\rangle, \end{aligned} \tag{72}$$

where Eq. (35) was used.

As discussed in Sec. XVII, fluctuations in particle number are negligible in the large-Ω limit for SO(8) coherent states, implying that the summations in Eq. (72) become dominated by terms with $p \simeq N$. Thus, for large Ω, the coherent state wave functions are well approximated up to a normalization by

$$|\mathrm{SO}_5 \times \mathrm{SU}_2\rangle \simeq (S^\dagger)^N |0\rangle, \tag{73a}$$

$$|\mathrm{SU}_4\rangle \simeq (Q_\pm^\dagger)^N |0\rangle. \tag{73b}$$

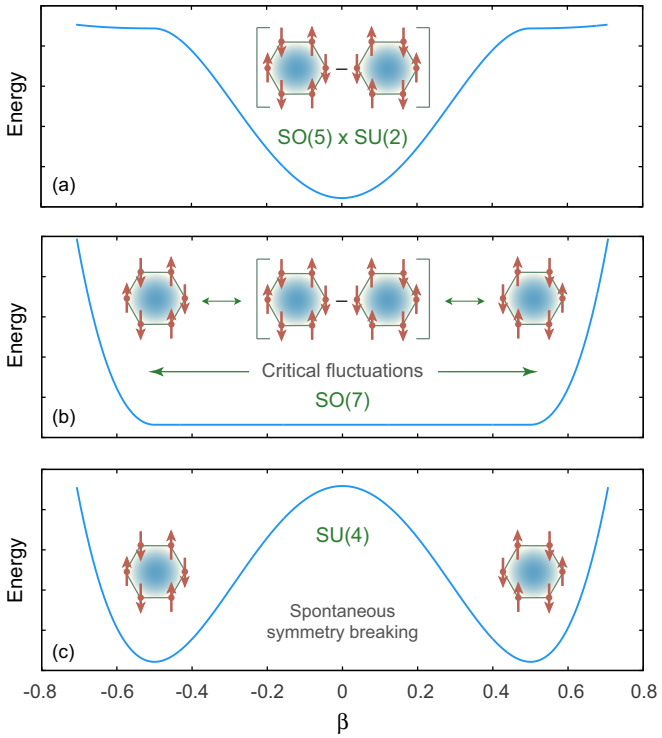

FIG. 12. Ground-state energy surfaces in coherent state approximation for three of the SO(8) dynamical symmetry limits. (a) The SO(5) × SU(2) limit. (b) The SO(7) limit. (c) The SU(4) limit. The diagrams indicate schematically the corresponding wave functions, as suggested by Eqs. (70)–(73) and Fig. 6.

As seen from Table III, the SU(4) state of Eq. (73b) is a coherent superposition of Q_- or Q_+ pairs, each contributing vanishing ferromagnetic order $\langle \mathcal{S}_z \rangle$ and charge density wave order $\langle T_z \rangle$, but nonzero AF order $\langle N_z \rangle$. Conversely, the SO(5) × SU(2) state of Eq. (73a) is a coherent superposition of S pairs, each with vanishing $\langle \mathcal{S}_z \rangle$, $\langle T_z \rangle$, and $\langle N_z \rangle$.

Thus the SO(5) × SU(2) and SU(4) limits of the SO(8) symmetry are distinguished by the order parameter $\langle N_z \rangle$, which is zero in the SO(5) × SU(2) state and is nonzero in the SU(4) state. Equivalently, the coherent state order parameter β vanishes in the pure SO(5) × SU(2) limit and is equal to $\pm\sqrt{n/4\Omega}$ in the pure SU(4) limit [see Eq. (64) and Fig. 11]. Equation (62) depends only on even powers of β so the sign for the two possible spontaneously broken symmetry solutions does not affect the energy.

For undoped graphene the Fermi surface corresponds to the $f = 0.5$ curves of Fig. 11. These are shown in Fig. 12 for the SO(5) × SU(2), SO(7), and SU(4) limits. (1) The SO(5) × SU(2) limit in Fig. 12(a) has its minimum β_0 at $\beta = 0$. It corresponds to states of the form (73a), with vanishing expectation values of $\mathcal{S}_z$, T_z, and N_z. (2) The SU(4) limit of Fig. 12(c) corresponds to states of the form (73b), with minima

located at

$$\beta_0 = \pm\sqrt{\frac{n}{4\Omega}} = \pm\frac{1}{2}.$$

When the symmetry is broken spontaneously by choosing one of these possibilities the resulting state has $\langle \mathcal{S}_z\rangle = \langle T_z\rangle = 0$ (no spin or isospin order), but $\langle N_z\rangle \neq 0$ (spin density wave or AF order). (3) The SO(7) limit of Fig. 12(b) corresponds to a critical dynamical symmetry that interpolates between the SO(5) × SU(2) and SU(4) states through critical fluctuations in the antiferromagnetic order. Thus the SO(8) dynamical symmetry limits illustrated in Fig. 12 represent a rich set of collective states that can be distinguished by the expectation value and fluctuations associated with the order parameter β.

XIX. SO(8) QUANTUM PHASE TRANSITIONS

The SO(8) coherent state solution can be used to study transitions among the phases defined in Fig. 12. For the $u = 0$ space (no broken pairs) assumed here, H' yields a constant that is neglected and Eq. (61) may be expressed as

$$H = G_0 S^\dagger S + b_2 P^2\cdot P^2 + b_3 C_{\mathrm{SO}(5)} + \frac{b_1 - b_3}{5} C_{\mathrm{SU}(2)}. \tag{74}$$

The last two terms yield constants when evaluated in a given representation, and $C_{\mathrm{SO}(5)}$ is found to contribute negligibly to the total energy compared with $C_{\mathrm{SU}(4)}$. Therefore it will be instructive to set $b_1 = b_3 = 0$ and study the approximate SO(8) Hamiltonian

$$H = G_0 S^\dagger S + b_2 P^2\cdot P^2. \tag{75}$$

From Table IV, one finds that

$$\langle S^\dagger S\rangle \sim \langle C_{\mathrm{SU}(2)}\rangle, \qquad \langle P^2\cdot P^2\rangle \sim \langle C_{\mathrm{SU}(4)}\rangle,$$
$$\langle S^\dagger S\rangle + \langle P^2\cdot P^2\rangle \sim \langle C_{\mathrm{SO}(7)}\rangle,$$

if constants are neglected. Thus the model Hamiltonian (75) may be tuned to favor the SO(5) × SU(2), SO(7), or SU(4) phases by varying the ratio of the coupling parameters G_0 and b_2.

A. Tuning quantum phase transitions

To study the quantum phase transitions of the SO(8) model with the approximate Hamiltonian (75), it is convenient to define a parameter $q \equiv b_2/G_0$ and to rewrite Eq. (75) as

$$H = G_0(S^\dagger S + q P^2\cdot P^2). \tag{76}$$

Thus the value of q tunes the Hamiltonian (76) between SU(2) × SO(5) and SU(4) phases via an intermediate SO(7) phase exhibiting quantum critical behavior. (1) If $q \ll 1$ the ground-state energy surface is approximated by Fig. 12(a), with a minimum at $\beta = 0$, no antiferromagnetic order, and SU(2) × SO(5) symmetry. (2) If $q \gg 1$ the ground-state energy surface is approximated by Fig. 12(c), with an energy minimum at $\beta \neq 0$ implying SU(4) symmetry and antiferromagnetic order. (3) If $q \sim 1$, the ground-state energy surface is approximated by Fig. 12(b) and the system exhibits SO(7) critical dynamical symmetry, with large fluctuations in the AF order parameter β. Let us now use the Hamiltonian (76) to study the quantum phase transitions and spontaneously broken symmetry of the SO(8) model.

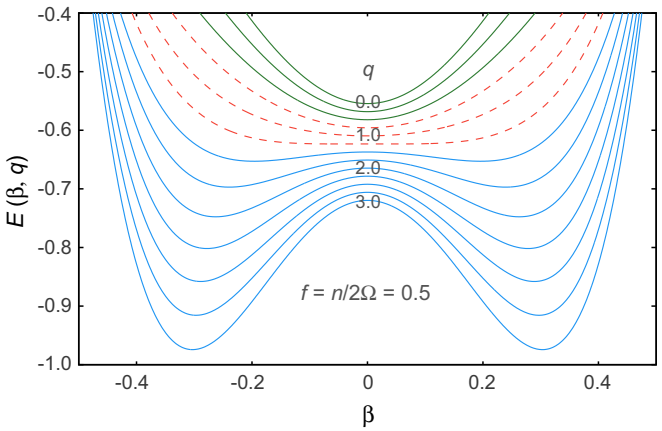

FIG. 13. Quantum phase transitions with coupling strength as control parameter: coherent state energy surface as a function of the control parameter $q \equiv G_0/b_2$ for a degeneracy parameter $\Omega = 50$ and a fractional occupation $f = n/2\Omega = 0.5$. The solid green curves from $q \sim 0$–0.5 correspond to approximate SO(5) × SU(2) symmetry, the solid blue curves for $q \geqslant 1.5$ correspond to approximate SU(4) symmetry. The dashed red curves near $q \sim 1$ correspond to an approximate SO(7) symmetry mediating the quantum phase transition from SO(5) × SU(2) to SU(4) symmetry.

B. Energy surfaces and quantum phase transitions

If terms involving $\langle P^1\cdot P^1\rangle$ and $\langle P^3\cdot P^3\rangle$ are ignored (as justified above), Eq. (62) with the parameters in Table V imply that

$$E_{\mathrm{SU}(2)} + E_{\mathrm{SU}(4)} - E_{\mathrm{SO}(5)} \simeq G_0\langle S^\dagger S\rangle + b_2\langle P^2\cdot P^2\rangle.$$

Hence the energy surfaces corresponding to the Hamiltonian (76) may be expressed as

$$\begin{aligned} E(n,\beta) = \langle H\rangle &= G_0\langle S^\dagger S\rangle + b_2\langle P^2\cdot P^2\rangle \\ &\simeq E_{\mathrm{SU}(2)}(n,\beta) + E_{\mathrm{SU}(4)}(n,\beta) - E_{\mathrm{SO}(5)}(n,\beta), \\ &\simeq E_{\mathrm{SU}(2)}(n,\beta) + E_{\mathrm{SU}(4)}(n,\beta). \end{aligned} \tag{77}$$

The variation of the energy surface computed from Eq. (77) with the control parameter $q = G_0/b_2$ for half-filling (ground state for undoped graphene) is shown in Fig. 13.

By tuning the control parameter from $q = 0$ to $q \gg 1$, one sees that the system undergoes a quantum phase transition near $q = 1$ from an approximate SO(5) × SU(2) state with energy minimum at $\beta = 0$ [see Fig. 12(a)] to an approximate SU(4) state having energy minima at $\beta = \pm(n/4\Omega)^{1/2}$ [see Fig. 12(c) and Eq. (64)]. For $q \sim 1$ the system has an approximate SO(7) dynamical symmetry [see Fig. 12(b)], with no well-defined minimum for the energy as a function of β, but with large fluctuations in β implied by a highly degenerate ground state.

For fixed values of the coupling parameters G_0 and b_2, phase transitions may be mediated by changing the particle occupancy. Figure 14 illustrates for different values of $n/2\Omega$ at fixed $b_2 = 2.5G_0$. One sees that as the particle number is increased the system makes a transition from approximate SO(5) × SU(2) symmetry with $\beta = 0$ to SU(4) symmetry with

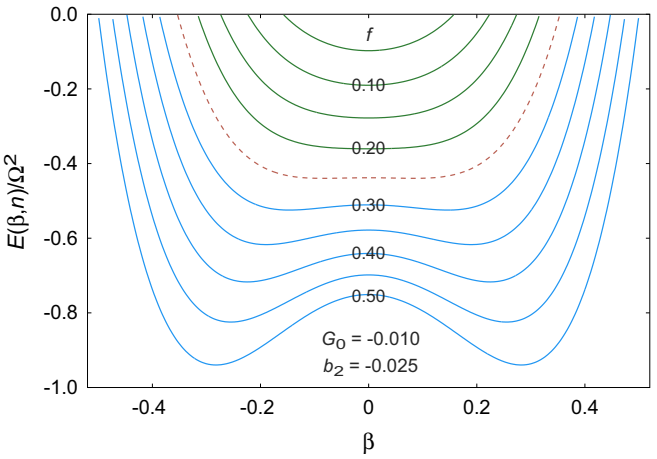

FIG. 14. Quantum phase transitions with particle number as control parameter: coherent state energy surfaces for different filling fraction $f = n/2\Omega$ at fixed values for G_0 and b_2 with $\Omega = 10{,}000$. The solid green curves for $n/2\Omega \sim 0$–0.2 correspond to approximate SO(5) × SU(2) symmetry, the solid blue curves for $n/2\Omega \sim 0.3$–0.5 correspond to approximate SU(4) symmetry. Curves near $n/2\Omega \sim 0.25$ (dashed red) correspond to an approximate SO(7) symmetry mediating the quantum phase transition from SO(5) × SU(2) to SU(4) symmetry.

$\beta \neq 0$ through a critical SO(7) symmetry for which the energy is highly degenerate in β.

XX. DISCUSSION

In the coherent state approximation, the dynamical symmetry structure of Fig. 10 has been examined and not the full group structure given in Fig. 8. For the group chains that contain the SO(5) subgroup, the only physical implication is to omit the effect of Zeeman splitting from dynamical symmetry Hamiltonian [which would break the SO(5) subgroup down into a U(1) subgroup generated by the z component of the physical spin]. Our primary concern in this discussion is the structure associated with the $n = 0$ Landau level, for which the effect of the Zeeman term is expected to be small (see Sec. XX). Thus one may view the effect of the Zeeman term as a perturbation on the results obtained thus far that will act only on the spin part of the wave function. As Kharitonov [26] has already discussed, the competition of the Zeeman term with the valley interactions will convert the antiferromagnetic solution into a canted antiferromagnetic solution.

The SU(4) symmetry of quantum Hall ferromagnetism gives rise to a ground state symmetry reflected in the SU(4)-symmetric Hamiltonian (5) and a possible symmetry breaking structure that has been outlined in Sec. VI. However, the symmetry-breaking patterns illustrated in Fig. 3 represents *perturbations around the symmetric ground state (explicit symmetry breaking)*. They cannot capture the nature of these possible spontaneously broken symmetry states, since the broken-symmetry states may differ fundamentally from the possible states in Fig. 3: the states corresponding to the most general linear combination (31) represent a complex superposition of many SU(4)-symmetric components and generally cannot be classified by pure or any simple linear combination of SU(4) irreducible representations. The broken-symmetry states have typically been studied numerically, or by effective field theory methods. However, as has been shown, the kinds of collective configurations that have been proposed as candidates for low-lying broken-symmetry states in graphene (see Fig. 6 and [26]) bear strong resemblance to *eigenstates* of SO(8) dynamical symmetry chains. Thus the present SO(8) symmetry holds the promise of providing *analytical* solutions for possible broken-symmetry states in graphene. This is the most important result of the present paper.

At specific filling factors the ground state of graphene will be determined by the competition among the SU(4) symmetry breaking terms. The most obvious SU(4)-anisotropic effect is the Zeeman term, which favors a spin-polarized state, but the graphene sublattice structure introduces additional interactions that favor ground states without spin polarization that are characterized by spin density wave or charge density wave order at the lattice scale. The competition between Zeeman-term spin polarization and the lattice-scale polarizations can be studied by changing the in-plane component of the magnetic field relative to the perpendicular component, since this changes the Zeeman energy but not the orbital energies [41]. Such studies indicate that for the higher-energy Landau levels the Zeeman term is dominant, producing spin ferromagnets that have skyrmionic excitations at half-filling, but in the $n = 0$ Landau level the lattice-scale interactions dominate the Zeeman interaction and drive the system into a spin-unpolarized state [42].

The remainder of this discussion will concentrate on these spin-unpolarized collective states that are candidates for the ground state in the $n = 0$ Landau level for charge-neutral graphene, with the Zeeman interaction viewed as a perturbation on a collective structure that is dominated by lattice-scale interactions. Consideration in this paper will be restricted further to those states that can arise from the dynamical symmetries of Fig. 8 that contain the SO(5) subgroup (those displayed in Fig. 10), with other states considered in future work.

It has been shown that SO(8) describes analytically a number of spontaneously broken-SU(4) candidates for the states observed in modern experiments such as those described in Refs. [9,10,41,42]. These solutions provide a spectrum of excited states as well as ground states. The excited states will not be discussed here, except to note that all ground state solutions have a gap to electronic and collective excitations and so correspond to incompressible states. The general theory to be discussed in forthcoming papers can accommodate FM, CDW, and AF states, but for the dynamical symmetries containing SO(5) that were the focus here, all solutions may be classified by a *single parameter* β measuring AF order: SU(4) states have finite AF order but no CDW or FM order, SO(5) × SU(2) states have no AF, CDW, or FM order, and SO(7) states correspond to a critical dynamical symmetry interpolating between SU(4) and SO(5) × SU(2) with large AF fluctuations but no static AF order, and with no CDW or FM order.

In a strong magnetic field, the zero-energy state of graphene has fourfold spin and valley degeneracy per Landau level, and (neglecting the lattice-scale interactions) near the sample

boundary one might expect the zero Landau level to split into one positively dispersing (electronlike) and one negatively dispersing (holelike) mode for each spin projection. This would suggest a ground state having a bulk energy gap at charge neutrality but with electronlike and holelike states of opposite spin polarization crossing at the edge of the sample (with the edge-state structure being analogous to the quantum spin Hall effect) [41,43,44]. However, experiments indicate that the ground state of charge-neutral graphene becomes *strongly insulating* at high magnetic fields [11]. The detailed nature of this state remains uncertain, but it is generally expected to correspond to a spontaneously broken symmetry caused by the strong Coulomb interactions among the electrons in the zero Landau level.

Transport properties are not manifest in the algebraic solutions presented here but the coherent state approximation is equivalent to symmetry-constrained Hartree-Fock-Bogoliubov (HFB) theory [32,40], suggesting that SO(8) theory can be mapped onto Hartree-Fock (HF) transport calculations. HF calculations for armchair nanoribbons found that AF and CDW states similar to ours have no edge currents [12]. It may be speculated that our AF states also are insulating and thus strong candidates for the high-field ground state, but confirmation requires more work.

Solutions depend on G_0 and b_2 in Eq. (75), which define effective interactions in the truncated space [highly renormalized relative to parameters in Eq. (5)]. They may be fixed by systematic comparison with data, enabling a robust prediction for the nature of the ground and other low-energy states. Modest impurity levels are expected to modify the effective interaction parameters but to leave dynamical symmetries intact. It may also be noted in this context that whereas it has been shown that graphene in a magnetic field, many collective nuclear states, and high-temperature cuprate superconductors can all exhibit SO(8) dynamical symmetry, one expects the fundamental differences between these systems to appear in their different effective interactions.

Finally, let us gather in one place the potential new capabilities and physics implied by the formalism introduced here. (1) The SO(8) dynamical symmetry chains reproduce the states expected from SU(4) quantum Hall ferromagnetism, but suggest that there are additional strongly collective states related to SU(4) states by quantum phase transitions that are not discussed in the previous literature but are potential ground states for graphene in a magnetic field. It is already clear that some of these states have unusual properties; for example, the SO(7) phase discussed further below. This qualitative statement can be turned into a quantitative one in future work by determining the effective interaction for the truncated space using the methodologies established in Refs. [16–20], which will permit expected experimental signatures to be calculated for these states.

(2) The SO(8) formalism predicts a spectrum of excited states for each of the possible ground states implied by the subgroup chains in Fig. 8. Is it possible to find experimental evidence for these either as discrete states, or as virtual intermediate states contributing to processes like scattering?

(3) As noted above, the predicted SO(7) subgroup chain is unusual. It represents a critical dynamical symmetry giving rise to a quantum critical phase. Evidence for such quantum critical phases has been found in heavy nuclei [34] and in high-temperature superconductors [19,20], where it is found that they produce systems exhibiting very strong complexity (extreme sensitivity to initial conditions) and fluctuatations [45]. These systems are described by dynamical symmetries having Lie algebras very similar to the graphene case. It will be of large interest to see whether such effects can be observed for graphene in strong magnetic fields.

(4) The global similarities among the Lie algebras describing collective states in high-temperature superconductors, heavy nuclei, and graphene in a magnetic field that was alluded to above suggests a deep mathematical analogy among these very different fields. There is no space to discuss this here but we note one interesting possibility: can these analogies be used to predict new behavior for graphene based on known behavior in nuclei and superconductors? One such analogy has already been suggested in previous work: the dynamical symmetry description of quadrupole collectivity in nuclei is analogous mathematically to the dynamical symmetry description of antiferromagnetism in high-temperature superconductors, which is in turn analogous mathematically to the dynamical symmetry description of the the lattice-scale "antiferromagnetic" states in graphene discussed in Sec. X A.

XXI. SUMMARY

The well-known quantum Hall ferromagnetic SU(4) symmetry of graphene in strong magnetic fields has been extended by adding to the particle-hole operators that generate SU(4) a set of six creation and six annihilation operators that create or destroy fermion pairs in either a total valley isospin triplet, total spin singlet state, or a total valley isospin singlet, total spin triplet state (the only possibilities allowed by the Pauli principle). This extended set of operators is shown to close an SO(8) algebra under commutation, which is formally analogous to the SO(8) algebra of the fermion dynamical symmetry model of nuclear structure physics. This permits immediate adaptation of mathematical tools developed in nuclear physics to the graphene problem.

The previously known SU(4) quantum Hall ferromagnetism symmetry is recovered as one subgroup, but one finds a richer set of low-energy collective modes associated with the full subgroup structure of SO(8). By exploiting the established methodology of fermion dynamical symmetries, it was possible to decouple a collective-pair subspace from the full Hilbert space of the problem, permitting exact, analytical, many-body solutions to be obtained in several physically interesting limits. In addition to exact solutions in specific dynamical symmetry limits, a generalized SO(8) coherent state approximation has been introduced that permits a broad range of solutions to be obtained even when not in the dynamical symmetry limits.

The pairs spanning the collective subspace are shown to be analogous to pairs that have already been discussed at a qualitative level in the graphene literature [26] as defining the possible broken-symmetry ground states in the presence of strong electron-electron and electron-phonon correlations in the $n = 0$ Landau level. The development here places these pairs on a firm, unified mathematical footing and permits analytical solutions to be developed that explore the possible

collective states that previously required numerical simulation for their quantitative description [26].

ACKNOWLEDGMENTS

This work is supported by the Basque Government (Grant No. IT986-16), the Spanish MICINN (Project No. FIS2015-69983-P), and the Basque Country University UFI (Project No. 11/55-01-2013). Partial support was provided by LightCone Interactive LLC.

APPENDIX: TRANSFORMATIONS BETWEEN BASES

This appendix collects some useful transformations among the several bases that have been employed in this paper. For brevity, in the following $\{P^1, P^2, P^3, S_0, S, S^\dagger, D_\mu, D_\mu^\dagger\}$ will be termed the nuclear SO(8) basis and $\{\mathcal{S}_\alpha, T_\alpha, N_\alpha, \Pi_{\alpha x}, \Pi_{\alpha y}, S_0, S, S^\dagger, D_\mu, D_\mu^\dagger\}$ will be termed the graphene SO(8) basis.

In transforming from the nuclear SO(8) basis to the graphene SO(8) basis the particle number (charge) operator n or S_0 and the 12 pairing operators $\{D_\mu, D_\mu^\dagger, S, S^\dagger\}$ are retained, but the 15 SU(4) generators $\{P^1, P^2, P^3\}$ in the nuclear representation are replaced with the 15 SU(4) generators $\{\mathcal{S}_\alpha, T_\alpha, N_\alpha, \Pi_{\alpha x}, \Pi_{\alpha y}\}$ defined in the graphene representation of Eq. (9). The explicit transformation from the $\{P^1, P^2, P^3\}$ generators to the $\{\mathcal{S}_\alpha, T_\alpha, N_\alpha, \Pi_{\alpha x}, \Pi_{\alpha y}\}$ generators is given by

$$\mathcal{S}_x = \sqrt{\frac{6}{5}}\left(P^1_{-1} - P^1_1\right) + \frac{2}{\sqrt{5}}\left(P^3_{-1} - P^3_1\right), \tag{A1a}$$

$$\mathcal{S}_y = i\left(\sqrt{\frac{6}{5}}\left(P^1_1 + P^1_{-1}\right) + \frac{2}{\sqrt{5}}\left(P^3_1 + P^3_{-1}\right)\right), \tag{A1b}$$

$$\mathcal{S}_z = \frac{2}{\sqrt{5}}P^1_0 + \frac{4}{\sqrt{5}}P^3_0 = n_1 - n_2 + n_3 - n_4, \tag{A1c}$$

$$T_x = -\sqrt{2}\left(P^2_2 + P^2_{-2}\right), \tag{A1d}$$

$$T_y = i\sqrt{2}\left(P^2_2 - P^2_{-2}\right), \tag{A1e}$$

$$T_z = \frac{4}{\sqrt{5}}P^1_0 - \frac{2}{\sqrt{5}}P^3_0 = n_1 + n_2 - n_3 - n_4, \tag{A1f}$$

$$N_x = \frac{1}{\sqrt{2}}\left(P^2_{-1} - P^2_1\right), \tag{A1g}$$

$$N_y = \frac{i}{\sqrt{2}}\left(P^2_{-1} + P^2_1\right), \tag{A1h}$$

$$N_z = P^2_0 = n_1 - n_2 + n_4 - n_3, \tag{A1i}$$

$$\Pi_{xx} = \frac{1}{2}\Bigg[P^3_{-3} - P^3_3 + \sqrt{\frac{2}{5}}\left(P^1_{-1} - P^1_1\right) + \sqrt{\frac{3}{5}}\left(P^3_1 - P^3_{-1}\right)\Bigg], \tag{A1j}$$

$$\Pi_{yx} = \frac{i}{2}\Bigg[\sqrt{\frac{2}{5}}P^3_{-3} + P^3_3 + \sqrt{\frac{2}{5}}\left(P^1_{-1} + P^1_1\right) - \sqrt{\frac{3}{5}}\left(P^3_1 + P^3_{-1}\right)\Bigg], \tag{A1k}$$

$$\Pi_{zx} = -\frac{1}{\sqrt{2}}\left(P^3_2 + P^3_{-2}\right) \tag{A1l}$$

$$\Pi_{xy} = \frac{i}{2}\Bigg[\sqrt{\frac{2}{5}}P^3_{-3} + P^3_3 - \sqrt{\frac{2}{5}}\left(P^1_{-1} + P^1_1\right) + \sqrt{\frac{3}{5}}\left(P^3_1 + P^3_{-1}\right)\Bigg], \tag{A1m}$$

$$\Pi_{yy} = \frac{1}{2}\Bigg[-P^3_{-3} + P^3_3 - \sqrt{\frac{2}{5}}\left(P^1_1 - P^1_{-1}\right) + \sqrt{\frac{3}{5}}\left(P^3_1 - P^3_{-1}\right)\Bigg], \tag{A1n}$$

$$\Pi_{zy} = -\frac{i}{\sqrt{2}}\left(P^3_2 - P^3_{-2}\right). \tag{A1o}$$

In Eqs. (17)–(20), the graphene basis $\{\mathcal{S}_\alpha, T_\alpha, N_\alpha, \Pi_{\alpha x}, \Pi_{\alpha y}\}$ has been expressed in terms of the generators B_{ab} defined in Eq. (15). The inverse transformations giving the B_{ab} in terms of the $\{\mathcal{S}_\alpha, T_\alpha, N_\alpha, \Pi_{\alpha x}, \Pi_{\alpha y}\}$ are

$$B_{12} = \frac{1}{2}N_x + \frac{1}{2}iN_y + \frac{1}{4}\mathcal{S}_x + \frac{1}{4}i\mathcal{S}_y, \tag{A2a}$$

$$B_{13} = \frac{1}{4}T_x + \frac{1}{4}iT_y + \frac{1}{2}\Pi_{zx} - \frac{1}{2}i\Pi_{zy}, \tag{A2b}$$

$$B_{14} = \frac{1}{2}\Pi_{xx} - \frac{1}{2}i\Pi_{yx} - \frac{1}{2}i\Pi_{xy} - \frac{1}{2}\Pi_{yy}, \tag{A2c}$$

$$B_{23} = \frac{1}{2}\Pi_{xx} + \frac{1}{2}i\Pi_{yx} - \frac{1}{2}i\Pi_{xy} + \frac{1}{2}\Pi_{yy}, \tag{A2d}$$

$$B_{24} = \frac{1}{4}T_x + \frac{1}{4}iT_y - \frac{1}{2}\Pi_{zx} + \frac{1}{2}i\Pi_{zy}, \tag{A2e}$$

$$B_{34} = \frac{1}{4}\mathcal{S}_x - \frac{1}{2}iN_y - \frac{1}{2}N_x + \frac{1}{4}i\mathcal{S}_y, \tag{A2f}$$

$$B_{11} = \frac{1}{4}\mathcal{S}_z + \frac{1}{4}T_z + \frac{1}{2}N_z + \frac{1}{4}(n - \Omega), \tag{A2g}$$

$$B_{22} = -\frac{1}{4}\mathcal{S}_z + \frac{1}{4}T_z - \frac{1}{2}N_z + \frac{1}{4}(n - \Omega), \tag{A2h}$$

$$B_{33} = \frac{1}{4}\mathcal{S}_z - \frac{1}{4}T_z - \frac{1}{2}N_z + \frac{1}{4}(n - \Omega), \tag{A2i}$$

$$B_{44} = -\frac{1}{4}\mathcal{S}_z - \frac{1}{4}T_z + \frac{1}{2}N_z + \frac{1}{4}(n - \Omega), \tag{A2j}$$

where the unlisted operators may be obtained from $B_{ba} = B_{ab}^\dagger$ and the diagonal operators have been assumed to obey the U(4) constraint

$$B_{11} + B_{22} + B_{33} + B_{44} = n - \Omega, \tag{A3}$$

with $n = n_1 + n_2 + n_3 + n_4$ the total particle number and Ω the total pair degeneracy given by Eq. (22).

Since from Eq. (46) the order parameters for the quantum Hall ground states are functions of the expectation values for the number operators n_a specifying the population of the four basis states in Table I and Fig. 4 labeled by the index a, it is

useful to have explicit expressions for them in terms of the P^r_μ operators. These are

$$n_1 = \frac{1}{4}n + \frac{3\sqrt{5}}{10}P_0^1 + \frac{1}{2}P_0^2 + \frac{\sqrt{5}}{10}P_0^3, \tag{A4a}$$

$$n_2 = \frac{1}{4}n + \frac{\sqrt{5}}{10}P_0^1 - \frac{1}{2}P_0^2 - \frac{3\sqrt{5}}{10}P_0^3, \tag{A4b}$$

$$n_3 = \frac{1}{4}n - \frac{\sqrt{5}}{10}P_0^1 - \frac{1}{2}P_0^2 + \frac{3\sqrt{5}}{10}P_0^3, \tag{A4c}$$

$$n_4 = \frac{1}{4}n - \frac{3\sqrt{5}}{10}P_0^1 + \frac{1}{2}P_0^2 - \frac{\sqrt{5}}{10}P_0^3, \tag{A4d}$$

where the total number operator n is

$$n = \tfrac{1}{2}N = n_1 + n_2 + n_3 + n_4 = 2\big(P_0^0 + \tfrac{1}{2}\Omega\big). \tag{A5}$$

[1] K. von Klitzing, G. Dorda, and M. Pepper, Phys. Rev. Lett. **45**, 494 (1980).
[2] R. B. Laughlin, Phys. Rev. B **23**, 5632 (1981).
[3] D. C. Tsui, H. L. Stormer, and A. C. Gossard, Phys. Rev. Lett. **48**, 1559 (1982).
[4] R. B. Laughlin, Phys. Rev. Lett. **50**, 1395 (1983).
[5] K. S. Novoselov *et al.*, Nature (London) **438**, 197 (2005).
[6] Y. Zhang *et al.*, Nature (London) **438**, 201 (2005).
[7] K. I. Bolotin, F. Ghahari, M. D. Shulman, H. L. Stormer, and P. Kim, Nature (London) **462**, 196 (2009).
[8] X. Du, I. Skachko, F. Duerr, A. Luican, and E. Y. Andrei, Nature (London) **462**, 192 (2009).
[9] B. E. Feldman, B. Krauss, J. H. Smet, and A. Yacoby, Science **337**, 1196 (2012).
[10] B. E. Feldman, A. J. Levin, B. Krauss, D. A. Abanin, B. I. Halperin, J. H. Smet, and A. Yacoby, Phys. Rev. Lett. **111**, 076802 (2013).
[11] J. G. Checkelsky, L. Li, and N. P. Ong, Phys. Rev. Lett. **100**, 206801 (2008).
[12] J. Jung and A. H. MacDonald, Phys. Rev. B **80**, 235417 (2009).
[13] I. F. Herbut, Phys. Rev. B **75**, 165411 (2007).
[14] I. F. Herbut, Phys. Rev. B **76**, 085432 (2007).
[15] B. Roy, M. P. Kennett, and S. D. Sarma, Phys. Rev. B **90**, 201409(R) (2014).
[16] C.-L. Wu, D. H. Feng, X.-G. Chen, J.-Q. Chen, and M. W. Guidry, Phys. Lett. B **168**, 313 (1986).
[17] C.-L. Wu, D. H. Feng, X.-G. Cheng, J.-Q. Chen, and M. W. Guidry, Phys. Rev. C **36**, 1157 (1987).
[18] C.-L. Wu, D. H. Feng, and M. W. Guidry, Adv. Nucl. Phys. **21**, 227 (1994).
[19] M. W. Guidry, L.-A. Wu, Y. Sun, and C.-L. Wu, Phys. Rev. B **63**, 134516 (2001).
[20] L.-A. Wu, M. W. Guidry, Y. Sun, and C.-L. Wu, Phys. Rev. B **67**, 014515 (2003).
[21] L.-A. Wu and M. W. Guidry, Sci. Rep. **6**, 22423 (2016).
[22] A. H. C. Neto, F. Guinea, N. M. R. Peres, K. S. Novoselov, and A. K. Geim, Rev. Mod. Phys. **81**, 109 (2009).
[23] M. O. Goerbig, Rev. Mod. Phys. **83**, 1193 (2011).
[24] T. Ando, T. Nakaishi, and R. Saito, J. Phys. Soc. Jpn. **67**, 2857 (1998).
[25] G. P. Mikitik and Y. V. Sharlai, Phys. Rev. Lett. **82**, 2147 (1999).
[26] M. Kharitonov, Phys. Rev. B **85**, 155439 (2012).
[27] F. Wu, I. Sodemann, Y. Araki, A. H. MacDonald, and T. Jolicoeur, Phys. Rev. B **90**, 235432 (2014).
[28] J.-Q. Chen, D. H. Feng, and C.-L. Wu, Phys. Rev. C **34**, 2269 (1986).
[29] B. G. Wybourne, *Classical Groups for Physicists* (Wiley Interscience, New York, 1974).
[30] For example, see D. M. Brink and G. R. Satchler, *Angular Momentum* (Clarendon Press, Oxford, 1968); or A. R. Edmonds, *Angular Momentum in Quantum Mechanics* (Princeton University Press, Princeton, 1959).
[31] J. N. Ginocchio, Ann. Phys. **126**, 234 (1980).
[32] W.-M. Zhang, D. H. Feng, C.-L. Wu, H. Wu, and J. N. Ginocchio, Nucl. Phys. A **505**, 7 (1989).
[33] F. Iachello and A. Arima, *The Interacting Boson Model* (Cambridge University Press, Cambridge, 1987).
[34] W.-M. Zhang, D. H. Feng, and J. N. Ginocchio, Phys. Rev. Lett. **59**, 2032 (1987).
[35] W.-M. Zhang, D. H. Feng, and J. N. Ginocchio, Phys. Rev. C **37**, 1281 (1988).
[36] F. T. Arecchi, E. Courtens, R. Gilmore, and H. Thomas, Phys. Rev. A **6**, 2211 (1972).
[37] R. Gilmore, Ann. Phys. **74**, 391 (1972).
[38] A. M. Perelomov, Commun. Math. Phys. **26**, 222 (1972).
[39] R. Gilmore, Rev. Mex. de Fisica **23**, 143 (1974).
[40] W.-M. Zhang, D. H. Feng, and R. Gilmore, Rev. Mod. Phys. **62**, 867 (1990).
[41] A. F. Young, J. D. Sanchez-Yamagishi, B. Hunt, S. H. Choi, K. Watanabe, T. Taniguchi, R. C. Ashoori, and P. Jarillo-Herrero, Nature (London) **505**, 528 (2014).
[42] A. F. Young, C. R. Dean, L. Wang, H. Ren, P. Cadden-Zimansky, K. Watanabe, T. Taniguchi, J. Hone, K. L. Shepard, and P. Kim, Nat. Phys. **8**, 550 (2012).
[43] D. A. Abanin, P. A. Lee, and L. S. Levitov, Phys. Rev. Lett. **96**, 176803 (2006).
[44] H. A. Fertig and L. Brey, Phys. Rev. Lett. **97**, 116805 (2006).
[45] M. W. Guidry, Y. Sun, and C.-L. Wu, Chin. Sci. Bull. **56**, 367 (2011).